An Insight into Characterizations and Applications of Nanoparticulate Targeted Drug Delivery Systems

11

Ayan Kumar Barui, Batakrishna Jana, and Ja-Hyoung Ryu

Contents

1 Definition of Topic 417
2 Overview 418
3 Introduction and Background 418
4 Experimental Methodology 419
4.1 Physicochemical Characterizations 420
4.2 Biological Characterizations 431
5 Therapeutic Applications of Drug Delivery Systems: Key Research Findings 439
5.1 Gold Nanoparticles 439
5.2 Silver Nanoparticles 440
5.3 Zinc Oxide Nanoparticles 441
5.4 Iron Oxide Nanoparticles 443
5.5 Titanium Oxide Nanoparticles 444
5.6 Carbon Nanotubes 445
5.7 Carbon Dots 446
5.8 Mesoporous Silica Nanoparticles 446
6 Conclusions: Challenges and Future Perspective 448
References 449

1 Definition of Topic

Nanoparticle-based targeted drug delivery system (DDS) is one of the major applications of nanotechnology in modern biomedical research. Basically, it comprises of bare or functionalized biocompatible nanoparticles with or without targeting ligands

Ayan Kumar Barui and Batakrishna Jana contributed equally with all other contributors.

A. K. Barui · B. Jana · J.-H. Ryu (✉)
Department of Chemistry, Ulsan National Institute of Science and Technology (UNIST), Ulsan, Republic of Korea
e-mail: jhryu@unist.ac.kr

C. S. S. R. Kumar (ed.), *Nanotechnology Characterization Tools for Tissue Engineering and Medical Therapy*, https://doi.org/10.1007/978-3-662-59596-1_11

and one or more chemotherapeutic drugs. While the targeting efficacy of DDS without targeting ligands involves passive targeting through enhanced permeability and retention (EPR) effect, DDS containing targeting ligands (e.g., protein, antibodies, peptides, and small molecules) relies on their specificity to cell surface receptors. To achieve combination therapy, two or more chemotherapeutic drugs (exhibiting synergistic effect) are often loaded on nanoparticulate DDS. Besides site-specific delivery, the release of drugs from the DDS and stability of nanomaterials are also important factors to develop an effective nanomedicine that could overcome the disadvantages (e.g., nonspecificity, less bioavailability, and adverse side effect) associated with conventional treatment strategies of different diseases. To comprehend the drug release, stability of nanomaterials as well as ultimate therapeutic applications of DDS, it is highly essential to gradually develop and understand relevant physicochemical and biological characterization techniques. In view of the rapid growth of modern biomedical research involving drug delivery, it might be speculated that many nanomedicines based on DDS would come up in near future for practical therapeutic applications in human.

2 Overview

Nanotechnology offers an extensive shift in modern days diagnostic as well as therapeutic treatment strategies for various types of diseases. The applications of nanotechnology are generally described as nanomedicine. The huge implication of nanomedicine for several disease theranostics might be manifested to the facile interaction of nanoparticles with cell surface receptors, proteins, DNA/RNA, and other biomolecules because of their nanoscale size similarity. Almost all of the conventional drugs for the treatment of some certain diseases have some common limitations such as side effect, nonspecificity issue, and low bioavailability. In this scenario, nanomedicine could play an important role through targeted drug delivery approach, where nanoparticles act as a drug carrier for the delivery of drugs to the specific disease site with better efficacy and reduced systemic toxicity. Although nanomedicine shows several biomedical applications, nanoparticle-based targeted drug delivery has got maximum attention to the researchers. Since past decades, numerous literature report only the applications of targeted drug delivery of different nanomaterials. However, the report describing the characterizations of drug delivery system (DDS) is very scarce. In this context, this chapter describes the detailed chemical and biological characterizations of nanoparticulate targeted DDS as well as their brief therapeutic applications. Finally, we conclude with diverse challenges and future aspects of nanoparticle-based targeted DDS.

3 Introduction and Background

Nanotechnology refers to an interdisciplinary field of contemporary science and technology encompassing the field of physics, chemistry, engineering, and biology [1–3]. It deals with various types of nanoparticles, having unique physicochemical characteristics

such as mechanical, electrical, optical, and biological properties as compared to the corresponding bulk substances, which could be attributed to their high surface area to volume ratio. Due to possessing unusual and interesting properties, nanomaterials exhibit various applications in diverse fields including agriculture, [4] energy, [5] catalysis, [6] electronics, [7] and environment [8]. Although nanotechnology involves numerous applications, it especially brings revolution in modern biomedical research field in terms of developing new therapeutic and diagnostic treatment strategies of different diseases via nanomedicine approach [9, 10]. The extensive applications of nanotechnology in healthcare research could be manifested by the easier interaction of nanoparticles with cell surface receptors (~10 nm), proteins (~1–20 nm), and nucleic acids (~2 nm) owing to their size (nanoscale range) similarity factor [9, 11].

Since past decades, scientists have highly engaged in design and development of various kinds of functionalized/engineered nanomaterials often called as nanocomposites for different therapeutic and diagnostic applications including cancer therapy, tissue engineering, wound healing, antimicrobial activity, bioimaging, and biosensor [9]. However, major reports related to the biomedical applications of nanocomposite systems demonstrate their potential for designing efficient drug delivery systems (DDSs), owing to their unique physicochemical features such as large surface area, high drug loading capacity, easier functionalization, and controlled drug release. The basic criteria for effective DDSs include slow and sustained release of therapeutic drugs as well as their delivery to the specific site of body system [12]. To achieve site-specific delivery of drug, researchers have generally employed either passive targeting or active targeting approaches [13]. While passive targeting strategy relies on enhanced permeability and retention (EPR) effect, [14] active targeting involves the conjugation of nanoparticles with some active ligands (e.g., recombinant proteins, peptides, antibodies, and small molecules) which would recognize cell surface receptors more specifically [15].

The most common nanocomposites employed for targeted drug delivery applications are based on noble metals (e.g., gold nanoparticles: AuNPs and silver nanoparticles: AgNPs), transition metal oxides (e.g., ZnO nanoparticles, TiO_2 nanoparticles, super paramagnetic iron oxide nanoparticles: SPIONs), carbon materials (e.g., graphene oxide: GO, carbon nanotubes: CNTs, carbon dots: CDs, etc.), silica (silica nanoparticles: SiNPs), lanthanides (cerium nanoparticles: CeNPs, gadolinium nanoparticles: GdNPs), as well as different organic/polymeric nanomaterials. Although various literature demonstrated the applications of targeted DDS, the reports related to the characterizations of DDS are very limited. In this circumstance, this chapter offers an overview of in-depth characterizations as well as brief therapeutic applications of recently developed nanoparticulate targeted DDS, which are described in the following sections.

4 Experimental Methodology

Proper characterization of nanoparticles is highly essential prior to their applications in any field especially in biomedical science and so for targeted drug delivery application. The physicochemical characterizations of nanoparticles for targeted

DDSs are based on their morphology, hydrodynamic size, surface charge, functionalization, stability, drug loading capacity, encapsulation efficiency, and drug release profile. On the other hand, biological characterizations for efficacy and mechanism of action of different DDSs include cellular uptake, cell viability assay, apoptosis assay, western blot, immunohistochemistry, and biodistribution. The following sections elaborately discuss the physicochemical as well as biological characterizations of nanoparticles and nanoparticulate targeted DDSs.

4.1 Physicochemical Characterizations

4.1.1 Analytical Techniques

There are various analytical techniques available for characterization of bare as well as functionalized nanoparticles such as transmission electron microscopy (TEM), scanning electron microscopy (SEM), atomic force microscopy (AFM), dynamic light scattering (DLS), X-ray diffraction (XRD), ultra violet spectroscopy (UV), Fourier-transform infrared spectroscopy (FT-IR), and nuclear magnetic resonance (NMR). While the morphology of nanomaterials is characterized by TEM, SEM, and AFM, the hydrodynamic size and surface charge of nanoparticles are characterized by DLS. TEM and DLS are also employed for the stability study of nanomaterials. XRD analysis provides the crystalline characteristics of nanoparticles. The functionalization of the nanoparticles is generally confirmed by FT-IR, NMR, and UV. Fluorimeter and UV spectroscopy are often employed for measuring the drug loading capacity and the encapsulation efficiency. The next sections elaborately discuss the characterization methodologies of nanoparticles and their DDSs.

4.1.2 Particle Size and Morphology

The nanoparticles are primarily characterized by their particle size distribution and morphology. The drug release from the nanoparticles is largely dependent on the particle size of the nanoparticle. Fast drug release is observed in case of small size nanoparticles due to their large surface area [16]. In contrast, slow diffusion of drug occurs when the drug is encapsulated inside the larger particles. Moreover, during the storage and transportation of the dispersed nanoparticles solution, there is a trend of aggregation in case of small size particles [16]. Therefore, there is a mutual compromise between the small size of the particles and maximum stability [17]. Also, extent of degradation of polymeric nanoparticles depends on the particle size, e.g., with increasing the particle size, the extent of poly (lactic-co-glycolic acid) degradation increases [18]. The surface morphology of the nanoparticles plays an important role in determining their stability for biological and biotechnological application. There are various analytical tools available for measuring the nanoparticle size as well the morphology as discussed below.

Dynamic Light Scattering (DLS)

DLS is very simple and widely used techniques for determination of the particle size. The size distribution profile of small Brownian particles in colloidal suspension in

nano or submicron ranges or polymer in solution is measured by DLS technique. When shining monochromatic light (laser) is exposed to solution of spherical particles in Brownian motion, Doppler shift occurs. There is a change in the wavelength of the incoming light as a result of hitting the monochromatic light with the moving particles. The size of the particles is determined by the extent of this change in wavelength. Various types of nanoparticles including polymers, micelles, lipid, proteins, carbohydrate, and inorganic nanoparticles are characterized by DLS. This measurement depends on the particle concentration, type of the ions in the medium, size of surface structures, and size of the particle core. DLS software of commercial instruments typically displays the particle population at different diameters. There is only one population in case of monodisperse solution. Multiple particle populations are observed in polydisperse systems. In 2012, Lee et al. developed a target-specific long-acting delivery system of interferon α (IFNα) for the treatment of hepatitis C virus (HCV infection). The authors have developed a hybrid material of AuNPs and hyaluronic acid (HA) for targeted delivery of interferon α (IFNα). IFNα was attached to HA-AuNPs through physical binding. Synthesis of HA-AuNP/IFNα complex was fully characterized by various spectroscopic techniques. The change in the particle size of AuNPs after attachment of HA and IFNα was measured by DLS. The mean hydrodynamic diameter of AuNPs was increased after HA and IFNα attachment (Fig. 11.1a) [19].

Transmission Electron Microscopy (TEM)

The most common technique to analyze the morphology, shape, and size of the nanoparticles is the TEM. Moreover, the aggregation tendency and the stability of the nanoparticles are often studied by TEM. It provides direct images of the nanoparticles and also accurate estimation of nanoparticle homogeneity. TEM is a microscopy technique based on the interaction between a thin sample and a uniform current density electron beam. When the electron beam reaches the sample, part of the electrons is transmitted, while the rest are scattered [20]. The magnitude of the interaction depends on several factors such as size, elemental composition, and sample density. The final images are produced with the information gathered from the transmitted electrons. Nanoparticle solution is deposited onto support grid or films during TEM characterization. To make nanoparticles unaffected against the instrument vacuum and easy handling, they are fixed using negative staining agent such as uranyl acetate and phosphotungstic acid. Alternatively, nanoparticle sample is exposed to liquid nitrogen temperatures after embedding in vitreous ice. One of the limitations of TEM is the difficulty in quantifying a large number of particles. Lee et al. used TEM for characterization of AuNP/IFNα and HA-AuNP/IFNα complex, used for targeted delivery of interferon α (IFNα) for the treatment of hepatitis C virus (HCV infection). The monodispersed morphology was observed in TEM images of AuNP/IFNα and HA-AuNP/IFNα complex (Fig. 11.1b) [19].

Scanning Electron Microscopy (SEM)

SEM is another type of electron microscope. The size, shape, and surface morphology of the nanoparticles with direct visualization is determined by this microscope. SEM

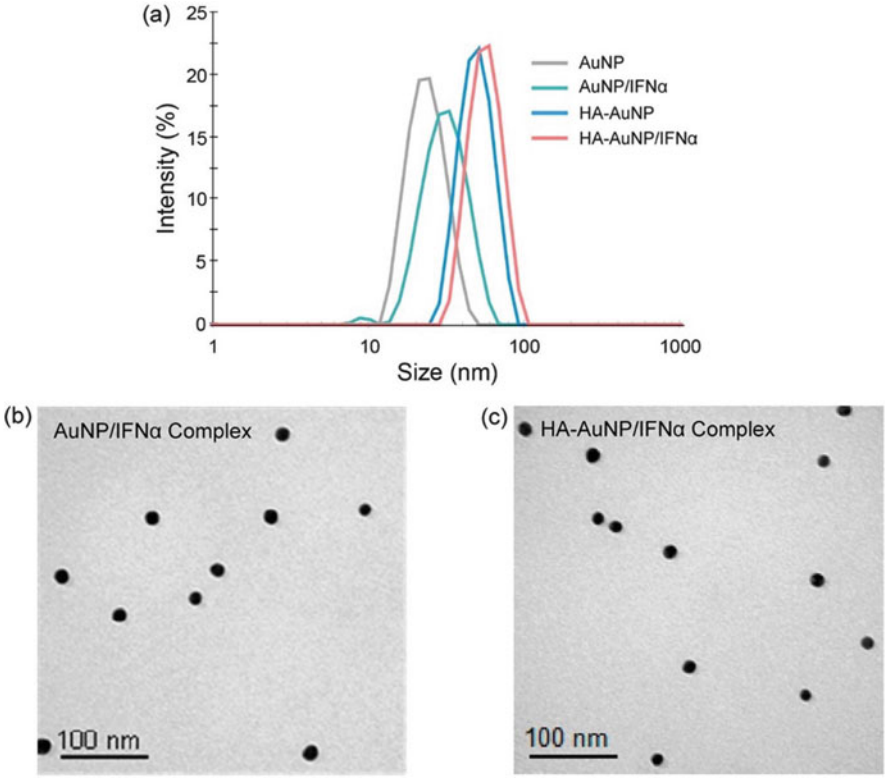

Fig. 11.1 (**a**) Dynamic light scattering analysis for the hydrodynamic diameter of AuNP/IFNα and HA-AuNP/IFNα complexes. Transmission electron microscopic images of (**b**) AuNP/IFNα and (**c**) HA-AuNP/IFNα complexes. (Adapted from Ref. [19]. Copyright © 2012, American Chemical Society)

constructs the images of the sample scanning its surface with a focused beam of electrons in a raster scan pattern. The surface topography and composition of the sample is obtained from the various signals, which is produced by the interaction of the electrons and the atoms in the sample. For nanoparticles characterization by SEM, the solution of nanoparticles should be converted into a dry powder. Then it will be further mounted on a sample holder and coated with conductive metal using a sputter coater. The whole sample is scanned with a focused fine beam of electrons [21]. The surface characteristics of the sample are determined by secondary electrons, emitted from the sample surface. The average mean size obtained from SEM and DLS is comparable. The disadvantages of this technique include high cost, time consuming process and frequent need of complementary information about size distribution [22]. In 2011, Sanpui et al. reported chitosan nanocarriers (NCs)-based delivery system, where the authors delivered silver nanoparticles (AgNPs) to mammalian cells. The authors observed that AgNP-nanocarriers (Ag-CS NCs) with very low concentrations of the

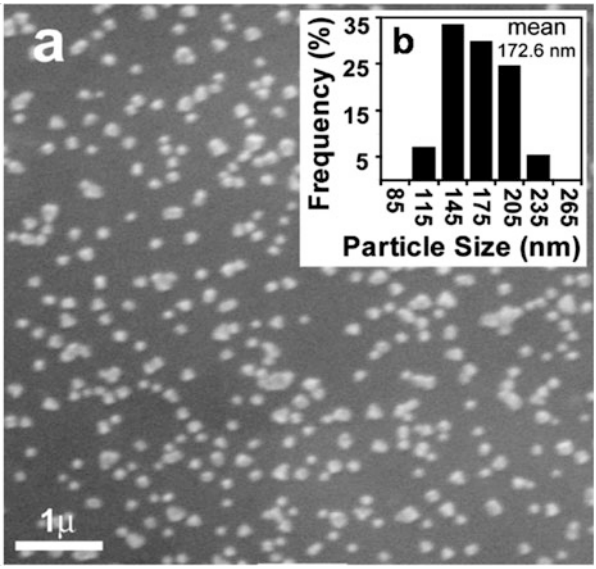

Fig. 11.2 (**a**) Typical SEM image of Ag-CS NCs. (**b**) (Inset) Particle size distribution calculated based on the SEM images and mean particle size was found to be 172.6 nm. (Adapted from Ref. [23]. Copyright © 2011, American Chemical Society)

AgNPs induces apoptosis to the mammalian cells. The average size and morphology of Ag-CS NCs was determined by SEM, which was found to be 172.6 nm (Fig. 11.2) [23].

Atomic Force Microscopy (AFM)

AFM is based on a physical scanning of samples at submicron level. A probe tip of atomic scale is required during AFM analysis. It offers ultrahigh resolution in particle size measurement [24]. This technique is also used for studying the particle size and morphology of the nanoparticles. The samples are generally scanned in contact mode or noncontact mode based on the properties of the samples. A topographical map is produced by tapping the probe on to the surface across the sample during contact mode; however, in noncontact mode, the probe drifts over the surface. The main advantage of AFM is, even nonconducting samples are imaged without any specific treatment. For that reason, delicate biological and polymeric nano- and microstructures also can be imaged [25]. The most accurate description of size, distribution of size, and real picture is obtained from AFM (without any mathematical calculation), which helps in understanding the effect of functionalization as well as various biological condition [26]. In 2010, Liu et al. developed a delivery platform based on PEGylated nanographene oxide for hydrophobic anticancer drug SN38 delivery. The authors characterized graphene oxide (GO) and PEGylated graphene oxide (NGO-PEG) by AFM. The as-made GO sheets were 50–500 nm in size, whereas NGO-PEG was ~5 to 50 nm. The researchers also checked the water and serum stability of GO and NGO-PEG. It was found that GO was aggregated in serum as well as in DMEM medium, but NGO-PEG was stable in those solutions (Fig. 11.3) [27].

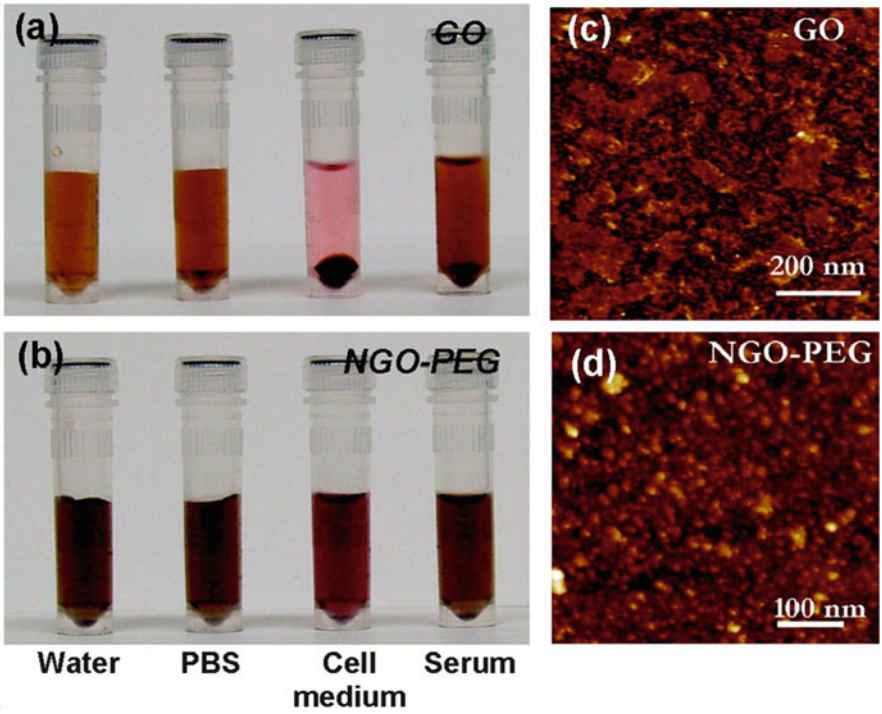

Fig. 11.3 PEGylation of graphene oxide: photos of GO (**a**) and NGO-PEG (**b**) in different solutions recorded after centrifugation at 10000*g* for 5 min. GO crashed out slightly in PBS and completely in cell medium and serum (top panel). NGO-PEG was stable in all solutions; AFM images of GO (**c**) and NGO-PEG (**d**). (Adapted from Ref. [27]. Copyright © 2008, American Chemical Society)

4.1.3 Surface Functionalization

Surface functionalization of the nanoparticles is very essential aiming various biomedical and biotechnological applications of inorganic, organic, and polymeric nanoparticles. The surface of the nanoparticles is functionalized with various molecules like PEGylation with polyethylene glycol for increasing the hydrophilicity and biocompatibility of the nanoparticles. The nanoparticles surface can also be functionalized with proteins, small molecules, peptides, various receptor targeting ligand, and anticancer drugs for various biomedical applications. After functionalization of nanoparticles, there is alteration in their size and surface morphology which are usually characterized by measuring the size distribution by TEM or DLS, and the surface charge by DLS. Most importantly, the functionalization of nanoparticles is generally characterized by various spectroscopic techniques such as UV-Vis spectroscopy, FT-IR, and NMR. Here we discuss the various spectroscopic techniques for characterization of functionalized nanoparticles.

UV-Vis Spectroscopy

One of the most important techniques for characterization of nanoparticles functionalization is UV-Vis spectroscopy. It is an absorption spectroscopy or reflectance spectroscopy in the ultra violet-visible spectral region. Absorption spectroscopy is complementary to fluorescence spectroscopy. Absorption measures transition from the ground state to the excited state, while fluorescence spectroscopy deals with transitions from the excited state to the ground state. Various nanoparticles have characteristic UV absorption peak, which is shifted to higher or lower wavelength or the intensity is lowered and increased after the functionalization. There is the appearance of new absorption peak or disappearance of exiting peak due to functionalization of nanoparticles in some cases. As discussed earlier, Lee et al. developed AuNPs-based DDS for targeted delivery of interferon α (IFNα) for the treatment of hepatitis C virus. The formation of AuNP/IFNα and HA-AuNP/IFNα complex was assessed by UV-Vis spectra. The surface plasmon resonance (SPR) band of AuNPs is red-shifted after attachment of IFNα, which confirms the interaction of IFNα with AuNPs. Moreover, the SPR peaks shifted from 519 to 523 and 527 nm as a result of stepwise binding of HA-SH and IFNα to AuNP (Fig. 11.4) [19].

FT-IR Spectroscopy

This is the most frequently used techniques for the characterization of functionalized nanoparticles. An infrared spectrum of absorption or emission of nanoparticles is obtained using FT-IR spectroscopy. An FTIR spectrometer simultaneously collects high-spectral-resolution data over a wide spectral range. The term Fourier-transform infrared spectroscopy implies that a Fourier transform (a mathematical process) is necessary to convert the raw data into the actual spectrum. There are some nanoparticles such as graphene and CNTs, which have characteristics FT-IR absorption peaks. There is shift in the FT-IR absorption peak position as well as appearance of the new peaks in the FT-IR spectrum of functionalized nanoparticles depending on the type of functionality present in the attached functional proof. FT-IR technique is the direct proof of the functionalization of nanoparticles.

NMR Spectroscopy

Since its discovery, NMR has grown to be one of the major characterization tool for scientists to obtain information about the structure and dynamics of molecules with atomic resolution. It has also important application in characterization of nanoparticles functionalization. It is a spectroscopic technique to observe local magnetic fields around atomic nuclei. An NMR signal is generated by excitation of the nuclei sample with radio waves into nuclear magnetic resonance, when the sample is placed in a magnetic field. The signal is detected with sensitive radio receivers. The intramolecular magnetic field around an atom in a molecule changes the resonance frequency. As a result, details of the electronic structure of a molecule and its individual functional groups are obtained. The synthesis of organic nanoparticles, polymeric nanoparticles, lipid nanoparticles, and micelle are usually confirmed by ^{1}H and ^{13}C NMR spectroscopy. NMR spectra of functionalized nanoparticles are

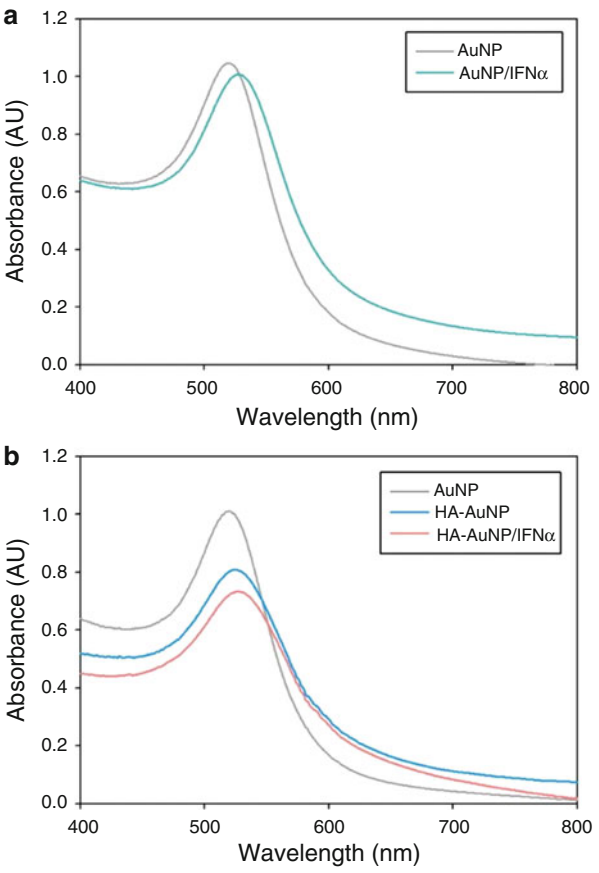

Fig. 11.4 UV-Vis spectra of (**a**) AuNP/IFNα and (**b**) HA-AuNP/IFNα complexes. (Adapted from Ref. [19]. Copyright © 2012, American Chemical Society)

changed due to different functionality and the interaction of the attached molecules with the nanoparticles. A novel gold conjugate (GNP-NHN = Dox-mPEG) with doxorubicin (DOX) shielded by PEGylation on the surface of GNPs is designed by Cui et al. [28] Fig. 11.5 represents the synthetic procedure of a novel lipoic acid (LA)-modified PEG derivative of Dox (LA-NHN = Dox-mPEG)-attached gold nanoparticles (GNP-NHN = Dox-mPEG) and their intracellular drug release mechanism. GNP-NHN = Dox-mPEG enters into the cancer cells through endocytosis mechanism followed by the liberation of Dox-mPEG in acidic lysosomes and then free Dox in cytoplasm, which is catalyzed by esterase.

The authors characterized the DDS GNP-NHN = Dox-mPEG through FT-IR and ^{1}H NMR spectroscopy (Fig. 11.6). All the data supports the successful synthesis of GNP-NHN = Dox-mPEG. A two-step stimulus-responsive drug release in response to an acidic environment in lysosomes and then esterase in the cytoplasm has been achieved with DOX-GNPs conjugate with improved solubility and stability, which allows sustained drug release to increase antitumor efficacy.

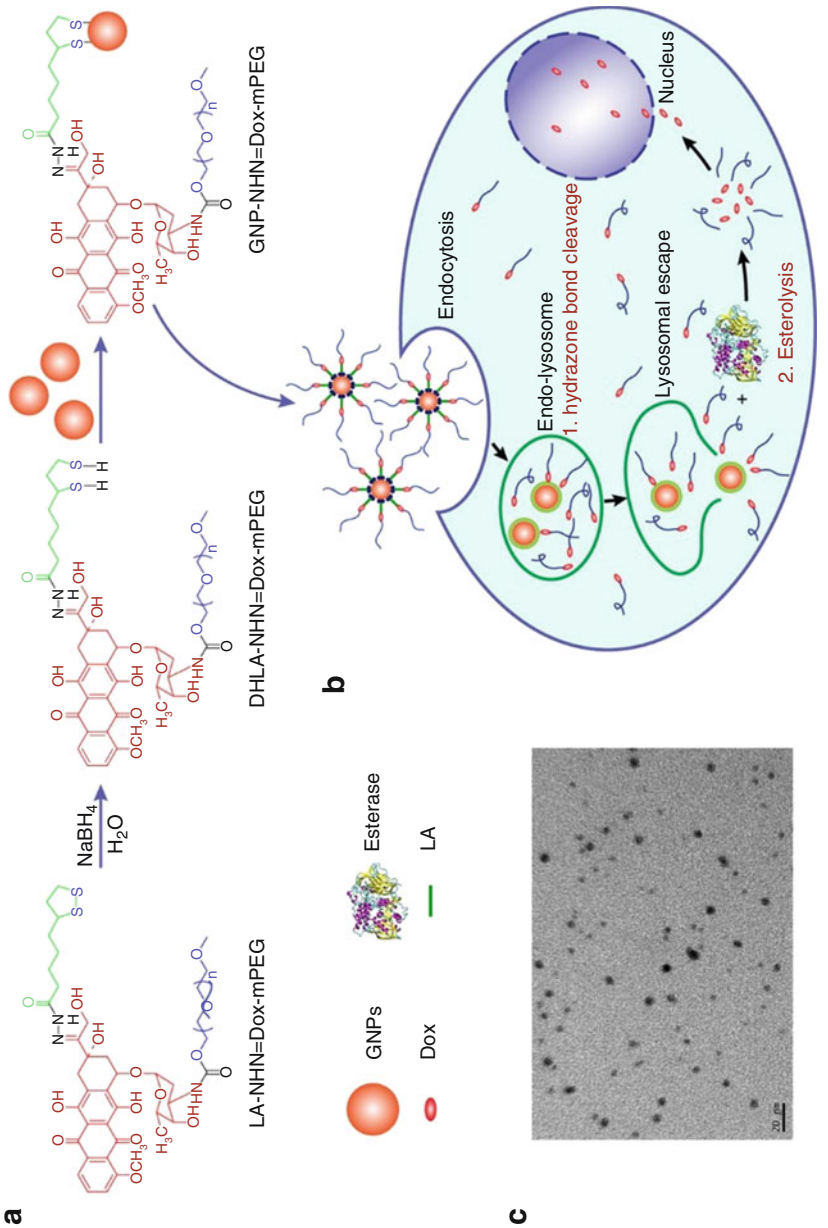

Fig. 11.5 (**a**) The structure of GNP-NHN = Dox-mPEG and (**b**) an illustration of its intracellular drug release mechanism. (**c**) TEM image of GNP-NHN = Dox-mPEG. The scale bar is 20 nm. (Adapted from Ref. [28]. Copyright © 2017, American Chemical Society)

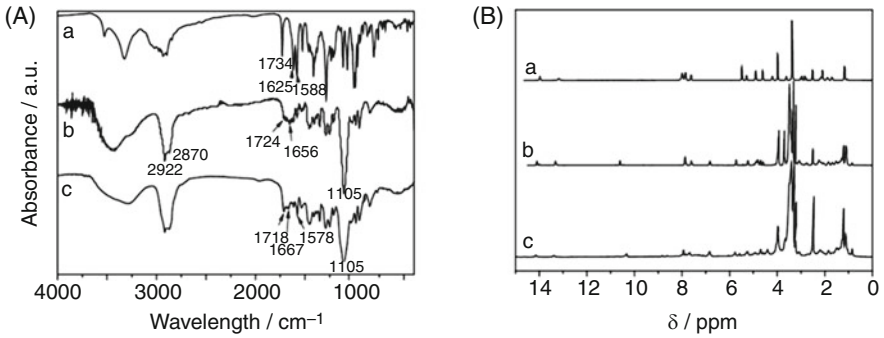

Fig. 11.6 (**A**) FT-IR spectra and (**B**) 1H NMR spectra of (*a*) Dox·HCl, (*b*) LA-NHN═Dox-mPEG, and (*c*) GNP-NHN═Dox-mPEG. (Adapted from Ref. [28]. Copyright © 2017, American Chemical Society)

4.1.4 Surface Charge

Interaction of nanoparticles with the bioactive molecules as well as with the biological environment is determined by their surface charge and intensity. Surface charge of the nanoparticle is estimated by measuring its zeta potential. Zeta potential of the nanoparticles determines the stability of colloidal materials. High zeta potential values (either positive or negative) of nanoparticles indicate the high stability and nonaggregation tendency. Moreover, the surface hydrophobicity, nature of the materials encapsulated within the nanoparticles, and type of materials coated or functionalized on the surface are also determined by measuring the zeta potential values [29]. Recently, Palanikumar et al. introduced a degradable mesoporous silica nanoparticle (MSN) system as a simple, facile, and versatile drug delivery vehicle, decorated with HA, which augmented the targeted delivery of doxorubicin hydrochloride to CD44 over-expressed cancer cells. The successful coating of polymeric gatekeeper as well as HA on the MSN was confirmed by measuring the zeta potential (Fig. 11.7) [30].

4.1.5 Drug Loading and Encapsulation Stability and Drug Release

A crucial property of nanoparticle-based therapeutic systems is drug release, directly related to the drug stability and the therapeutic results. It is a process by which the drug loaded in or on the nanomaterials is released in the body through diffusion or dissolution of the nanomaterials matrix releasing the drug in solution or the release of the drug from the nanoparticles by biodegradation, a process of breakdown of the DDSs inside the body. One should consider both the drug release and biodegradation during the development of nanoparticle-based DDS. Generally, the effectiveness of drugs not only depends on its active component, but its diffusion and solubility. The effectiveness of the nanoparticle-based drug delivery is affected by the particle size and the release process, which is again affected by the biodegradation of the particle matrix. Faster rate of drug release is observed in case of smaller particles as it has large surface area to volume ratio, so most of the drug molecules will be near the

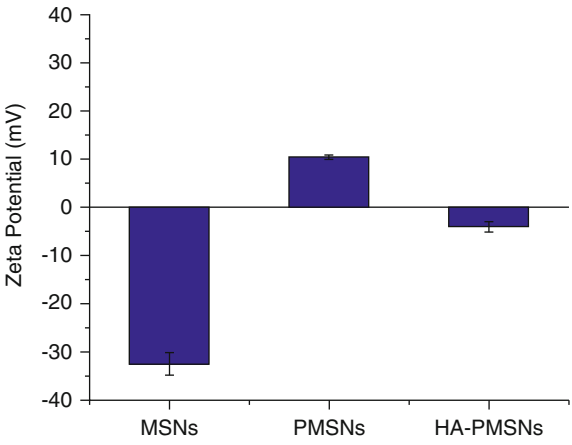

Fig. 11.7 Zeta potential measurement for MSNs, PMSNs, HA-PMSNs. (Adapted from Ref. [30]. Copyright © 2018, American Chemical Society)

particle surface. In contrast, in case of larger size particles, slower drug release is observed as its larger core allows more drugs to be encapsulated per particles. Therefore, particle size is an important factor to consider during design of nanoparticle-based DDS. There are two important parameters "drug loading capacity" and "drug entrapment efficiency," which determine the capacity of DDS. Drug loading capacity denotes the mass of the drug encapsulated in the nanoparticles/mass of the nanoparticles, whereas drug entrapment efficiency denotes mass of the loaded drug/mass of initial drug. Various techniques such as high-performance liquid chromatography (HPLC) after ultracentrifugation, gel-filtration, ultra-filtration, and UV spectroscopy are used to measure these parameters. Similar techniques for determination of drug loading are also used for drug release analysis, which is generally assessed for a period of time to evaluate the drug release mechanism [31, 32]. In general, release rate of the drug depends on several factors such as desorption of the surface bound or adsorbed drug, drug solubility, nanomaterials matrix degradation or erosion, and drug diffusion out of the nanomaterials matrix. When the drug is loaded to the nanoparticle through covalent attachment, the drug release is affected completely by drug-nanomaterials diffusion. When the drug is encapsulated inside nanomaterials, diffusion of the drug from the nanomaterials interior controls the drug release. In an encapsulated drug where the drug is uniformly distributed inside the nanomaterials matrix, drug release occurs by diffusion and/or erosion of the matrix. The diffusion largely controls the mechanism of release, when the diffusion of the drug is faster than matrix erosion. Recently, various DDSs have been reported, where the drug release is controlled by external stimuli such as light, pH, and enzyme. In 2013, Wang et al. developed dendrimer-encapsulated gold nanoparticles (DEGNPs) as a carrier of thiolated anticancer drugs. Thiol-containing drugs such as captopril and 6-mercaptopurine loaded within DEGNPs showed an "off−on" release behavior in the presence of thiol-reducing agents such as glutathione and dithiothreitol (Fig. 11.8) [33].

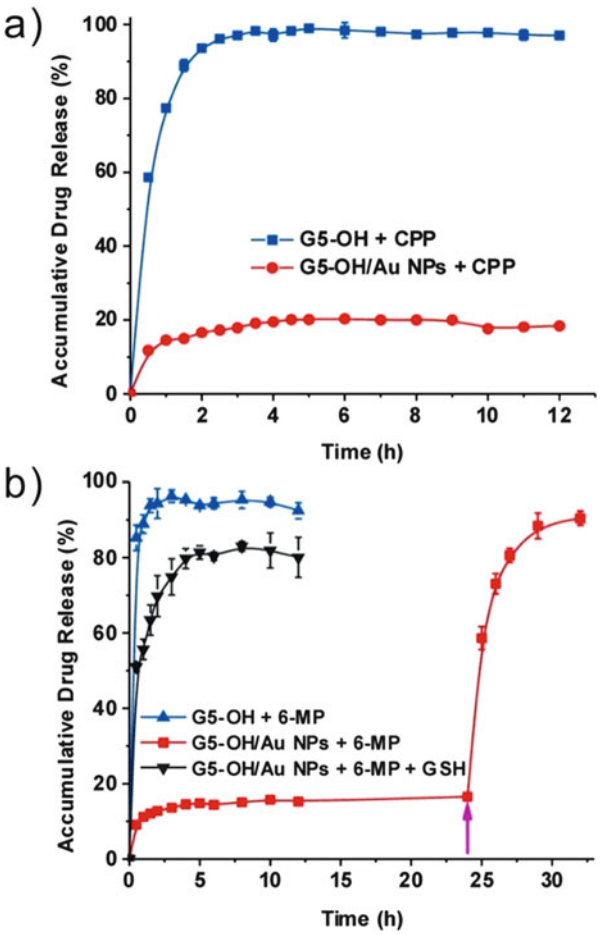

Fig. 11.8 In vitro release profiles of CPP (**a**) and 6-MP (**b**) from G5-OH and G5-OH/Au NPs. The purple arrow (**b**) indicates the addition of DTT into the complex solution at 24 h. (Adapted from Ref. [33]. Copyright © 2013, American Chemical Society)

4.1.6 Nanoparticle Stability

Stability of the nanoparticles is measured by the DLS. Aggregation tendency of the nanoparticles over time can be measured by measuring the size of the nanoparticles in DLS over time. If there is aggregation of the nanoparticles, there will be larger population of particles with larger radius and size of the nanoparticles will increase with time. In contrast, there will be no change in the particle size in case of the stable nanoparticles. Stability of the nanoparticle plays a critical role in determining their potential application in drug delivery. There are two terms "colloidal stability" and "serum stability" most frequently used to address the stability of the nanoparticles. When a nanoparticle is added to the biological medium such as phosphate buffer saline (PBS) and Dulbecco's modified Eagle's medium (DMEM), their intrinsic properties such as surface charge, size, and aggregation state could change significantly due to interaction with the physicochemical properties of the solution such as pH, components, and temperature. These properties of the nanoparticle determined

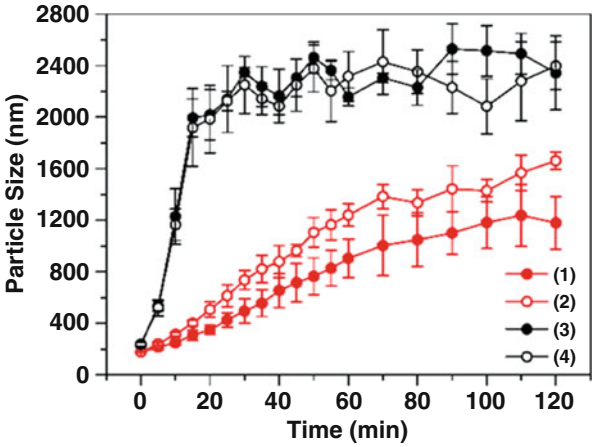

Fig. 11.9 Particle sizes of SFNPs prepared with acetone or ethanol as a function of time in serum-free DMEM or 0.01 mol/L PBS. (1) SFNPs prepared with acetone in serum-free DMEM; (2) SFNPs prepared with acetone in 0.01 mol/L PBS; (3) SFNPs prepared with ethanol in serum-free DMEM; and (4) SFNPs prepared with ethanol in 0.01 mol/L PBS. (Adapted from Ref. [34]. Copyright © 2015, American Chemical Society)

the colloidal stability of nanoparticles. Such properties of the nanoparticles do not change in case of the nanoparticle which have good colloidal stability. However, poor colloidal stability makes the nanoparticle unsuitable for drug delivery application. There is another term, i.e., serum stability, which signifies the stability of the nanoparticle in blood serum. The nanoparticle must remain unchanged and circulate in the blood for a moderately long period of time after intravenous injection to be accumulated at the target site, to be used as a potential drug delivery candidate. In 2015, Wang et al. reported the increase in colloidal stability of silk fibroin nanoparticles after coating with cationic polymer for effective drug delivery application. The authors checked the colloidal stability of their nanoparticles by measuring the change in the particle size by DLS over time (Fig. 11.9) [34].

4.2 Biological Characterizations

4.2.1 Cell Viability Assay

Cell viability assay is one of the fundamental assays to comprehend the biocompatibility of the nanoparticles, and therapeutic efficacy of these biocompatible nanoparticulate targeted DDS in vitro [35–40]. To perform cell viability assay, researchers have used various reagents including MTT (3-(4, 5-dimethylthiazol- 2-yl)-2, 5-diphenyl tetrazolium bromide), alamarBlue, and trypan blue. In MTT reagent-based cell viability assay, yellow-colored MTT is reduced by the mitochondrial dehydrogenase present in the cells, leading to the formation of purple formazan crystals, whose absorbance could reflect the viable cells [35, 36]. On the other hand, nonfluorescent alamarBlue reagent (resazurin-based blue-colored solution) is getting reduced upon entering into live cells leading to the formation of red fluorescent resorufin, whose absorbance or fluorescence can reflect the cell viability. Trypan blue dye is also used for determining the cell viability, where the principle is that living cells can exclude the trypan blue dye due to their intact membrane, while dead cells cannot.

Among all these reagents described above, MTT reagent has most frequently been used for checking the cell viability in presence of any materials and so for nano-conjugated system [35–40]. To perform cell viability assay, cells (generally, 10,000 cells/well) are seeded in all the wells of 96-well tissue culture plate and kept inside a humidified incubator system (37 °C, 5% CO_2) for 24 h. The cells are then treated with the nanoparticles and/or DDS at different concentrations for a certain period of times (generally, 24–72 h). After this, media in the wells are replaced by DMSO-MeOH (1:1; v/v) mixture to solubilize the purple formazan crystals, followed by checking the absorbance of the purple solution in each well of the plate using a multimode reader at 570 nm. The cell viability in presence of the treatment materials can be normalized by considering the viability of untreated control cells as 100%. For example, Bollu et al. developed MSU-2 as well as MCM-41-based chloro- and amine-functionalized SiNPs containing anticancer drug curcumin [35]. Cell viability study using MTT reagent (Fig. 11.10) demonstrated that the curcumin-loaded DDSs (MSU-2: **V3** and MCM-41: **V6**) exhibited more inhibition of cancer cells (A549, MCF-7, and B16F10)

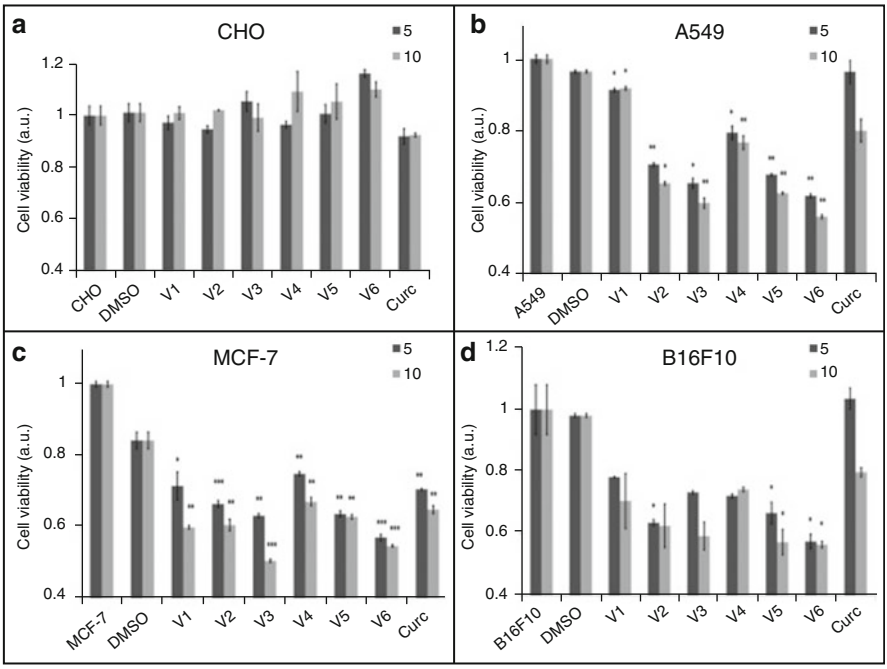

Fig. 11.10 Cell viability assay in normal (CHO) and cancerous (A549, MCF-7, B16F10) cell lines incubated with **V1-V6**. (**a**) All the materials (**V1-V6**), including curcumin-loaded materials, exhibit their biocompatible nature into CHO cells. (**b**–**d**) Curcumin-based nanostructured **V3** and **V6** materials show significant cytotoxicity in various cancer cells [A549 (**b**), MCF-7 (**c**), and B16F10 (**d**)] compared to pristine curcumin suggesting the materials as potent drug delivery systems. Curcumin and DMSO have been used as positive and vehicle control experiments, respectively. Numerical values 5 and 10 indicate doses in μM with respect to curcumin. $^{*}P \leq 0.05$, $^{**}P \leq 0.005$, $^{***}P \leq 0.0005$ compared to control. (Adapted from Ref. [35]. Copyright © 2016, Royal Society of Chemistry)

proliferation in a dose-dependent manner as compared to untreated control cells, corresponding chloro- (MSU-2: **V1** and MCM-41: **V4**), and amine (MSU-2: **V2** and MCM-41: **V5**)-functionalized SiNPs as well as free curcumin. However, all the SiNPs-based materials (**V1**-**V6**) are found to be biocompatible in normal CHO cells. Overall, the cell viability study depicted the therapeutic potential of the SiNPs-based DDSs **V3** and **V6**.

4.2.2 Cellular Internalization

Cellular internalization of nanomaterials and corresponding DDS is another basic assay to rationalize their mode of actions. Cellular uptake of nanopartiulate DDS have often been characterized by means of several techniques including fluorescence/confocal microscopy, flow cytometry, TEM, and ICP-OES/ICP-MS [35, 36]. In case of fluorescence/confocal microscopy and flow cytometry-based cellular uptake characterizations of DDS, the nanoparticles or therapeutic drug should possess inherent fluorescence properties that could be detected by the respective instruments. For instance, Bollu et al. synthesized curcumin-loaded functionalized SiNPs-based DDSs (**V3** and **V6**) as described in earlier section and studied the kinetics of internalization of **V3** and **V6** in A549 cells through fluorescence microscopy exploiting the inherent green fluorescence of curcumin [35]. The result exhibited that **V3**- and **V6**-treated cells showed more green fluorescence as compared to untreated control cells, and the intensity of green fluorescence was enhanced with time (Fig. 11.11). The result suggested that intracellular uptake

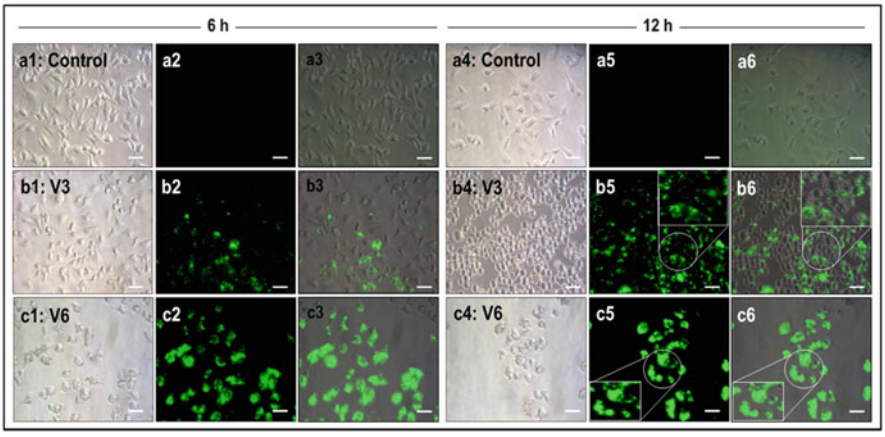

Fig. 11.11 Investigation of intracellular uptake of **V3** and **V6** in A549 cells using fluorescence microscopy. Kinetic study for cellular internalization using fluorescence microscopy shows that the cellular uptake of curcumin-loaded materials **V3** and **V6** increases in a time-dependent manner as indicated by the enhanced green fluorescence intensity with time. Row1: control (a1–a3: 6 h; a4–a6: 12 h); Row 2: cells treated with **V3** (b1–b3: 10 μM w.r.t. curcumin, 6 h; b4–b6: 10 μM w.r.t curcumin, 12 h); Row 3: cells treated with **V6** (c1–c3: 10 μM w.r.t. curcumin, 6 h; c4–c6: 10 μM w.r.t. curcumin, 12 h). Column 1 and Column 4: bright field images; Column 2 and Column 5: green fluorescent images; Column 3 and Column 6: merging of bright field and green fluorescent images. The inset picture shows the enlarged images of cellular fluorescence. Scale bar = 50 μm. (Adapted from Ref. [35]. Copyright © 2016, Royal Society of Chemistry)

of **V3** and **V6** was increased with time. This cellular uptake study was further confirmed by flow cytometry as well as ICP-OES analysis.

When the nanoparticles and the drug do not have fluorescence characteristics, some dyes (e.g., DiI, FITC, Rhodamine, Cyanine, etc.) have often been conjugated with the nanoparticulate DDS so that their internalization can be monitored either through fluorescence/confocal microscopy or flow cytometry instrument. The kinetic study of internalization of the DDSs could even be performed by these techniques by incubating the cells with DDSs for different time points. It is to be mentioned here that the cells could be live or fixed using paraformaldehyde (PFA) for fluorescence/confocal microscopy experiment. However, the cells are trypsinized after treatment followed by washing with Dulbecco's phosphate-buffered saline (DPBS) and then analyzed with flow cytometry instrument. Besides microscopy and flow cytometry, TEM have often been employed to analyze treated cells for understanding the localization of nanoparticulate system inside cells, whether in cytoplasm or nucleus. ICP-OES and ICP-MS techniques are also used to determine the cellular internalization of DDSs in terms of the content of respective elements present in nanoparticles.

4.2.3 In Vitro Mechanistic Study

To understand the mechanistic pathways for therapeutic efficacy of DDSs, scientists have employed several methodologies including apoptosis assay, determination of reactive oxygen species (ROS), immunocytochemistry, and western blot, which are briefly described in this section.

Scientists have often employed apoptosis assay to understand whether a material-based toxicity to cells are induced via apoptosis pathway [35, 36, 39]. Apoptosis assay for nanoparticulate DDSs are carried out either through propidium iodide (PI)/Hoechst staining-based fluorescence microscopy or by means of flow cytometry analysis. PI (DNA binding dye) can stain more the damaged DNA of nucleus during late apoptosis process. In case of microscopy method, the cells are generally treated with DDSs for a certain time period, followed by fixation with PFA and permeabilization using triton-X. The cells are then incubated with PI/Hoechst solution for some periods, washed with DPBS, and analyzed through fluorescence/confocal microscopy. On the other hand, for flow cytometry technique, after the respective treatments with DDS, the cells are washed with DPBS and stained with Annexin V FITC and PI staining solution, followed by analysis in flow cytometry instrument.

ROS plays an important role for various cellular signaling pathways. Therefore, researchers often check whether DDSs could induce the formation of intracellular ROS such as H_2O_2 or O_2^- using fluorescence/confocal microscopy technique [35, 36]. To measure the generation of intracellular ROS, cells are first treated with nanoparticulate DDS, followed by staining with either H_2DCFDA (green fluorescence for H_2O_2) or DHE (red fluorescence for O_2^-) and then analyzed with fluorescence/confocal microscopy. The cellular esterase could cleave the acetate group of H_2DCFDA, which can get oxidized by DDS-induced intracellular H_2O_2, leading to the formation of green fluorescent DCF (2′,7′-dichlorofluorescein), that could be detected through fluorescence/confocal microscopy [38]. On the other hand, the formation of intracellular O_2^- could be

assessed by observing the red fluorescence deriving from the reaction of DDS-induced O_2^- and DHE, leading to the generation of 2-hydroxyethidium (red fluorescent). For instance, Kotcherlakota et al. developed KIT-6 (**S2**), MSU-2 (**S4**), as well as MCM-41 (**S6**) based functionalized SiNPs conjugated with anticancer drug curcumin and demonstrated the efficient antiproliferative effect of all these DDSs, especially **S4** to various cancer cells (A549, MCF-7 and SKOV3) as compared to free curcumin [36]. The authors employed fluorescence microscopy study (Fig. 11.12) using DHE reagent, which revealed that all these DDSs (**S2**, **S4**, and **S6**), especially **S4**, induced intracellular formation of O_2^- (evidenced by red fluorescence) as compared to the untreated control cells and corresponding functionalized SiNPs without drug attachment (**S1**, **S3**, and **S5**). The result indicated that formation of ROS might play a crucial role underlying therapeutic potential of the DDSs.

Immunocytochemistry has been used by various researchers to understand the expression of different proteins in cells treated with nanomedicine. These proteins are

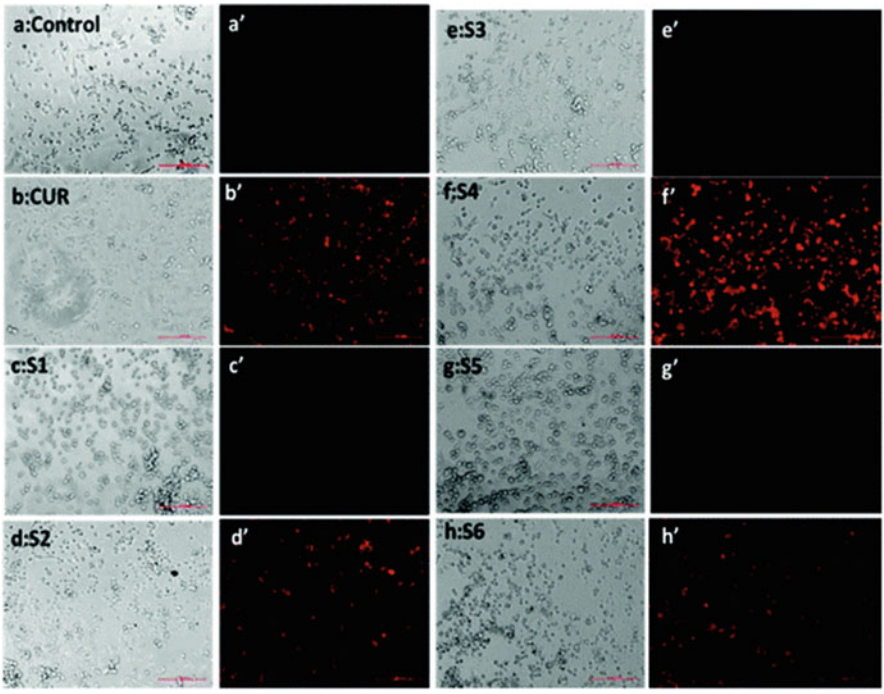

Fig. 11.12 Determination of intracellular superoxide anion radicals in A549 cells by fluorescence microscopy. The results show the formation of the superoxide ion radical in cells treated with curcumin-loaded materials. Phase images (**a**–**h**) and corresponding fluorescent images (**a'**–**h'**) of A549 cells. (**a**–**a'**): untreated control cells; (**b**–**b'**): cells treated with curcumin (10 μM); (**c**–**c'**): cells treated with **S1**; (**d**–**d'**): cells treated with **S2**; (**e**–**e'**): cells treated with **S3**; (**f**–**f'**): cells treated with **S4**; (**g**–**g'**): cells treated with of **S5**; (**h**–**h'**): cells treated with **S6**. The doses of all curcumin-loaded silica materials are 10 μM w.r.t. curcumin. Scale bar = 200 micron. (Adapted from Ref. [36]. Copyright © 2016, Royal Society of Chemistry)

often responsible in regulating the cellular mechanism which plays important role in the therapeutic efficacy of the nanomedicine. The cells are generally seeded on coverslips, and after the treatment with nanomedicine, the cells are washed with DPBS, fixed with PFA, and permeabilized with triton-X. The cells are then subjected to blocking using BSA in TBST buffer, followed by incubation with primary antibody and fluorescence moiety conjugated secondary antibody sequentially for certain time periods. The coverslips are mounted with DAPI for nucleus staining and sealed using nail polish, followed by analyzing through fluorescence/confocal microscopy.

Similar to immunocytochemistry, expression of different proteins responsible for cell signaling cascades are often been investigated using western block technique. To perform western blot, the cells are first incubated with nanomedicine for certain time periods. The cells are then lysed employing RIPA buffer (radioimmune precipitation assay buffer) which contains protease inhibitor cocktail [35, 36]. To get the cell lysate, the cell suspension are centrifuged, followed by estimation of protein content in lysate using Bradford assay or BCA assay. The equal amount of proteins is loaded on SDS-polyacrylamide gel and blotted on PVDF or nitrocellulose membrane after separation through electrophoresis. The proteins are blocked using BSA or nonfat dry milk and incubated with primary and secondary antibodies sequentially for some periods. The blot is then developed using colorimetric or chemiluminescence reagents to understand the expression of the target proteins. For instance, Kotcherlakota et al. developed functionalized SiNPs-based curcumin-loaded DDS (**S4**) as described in earlier section and studied the mechanism of therapeutic potential of the DDS through western blot analysis [36]. The result revealed that **S4** treatment in A549 cancer cells led to downregulation of the expression of poly ADP ribose polymerase (PARP) protein as compared to control experiment and corresponding amine-functionalized SiNPs (Fig. 11.13**)**. The result suggested that **S3** exhibited cancer therapeutic potential by inducing apoptosis in cancer cells.

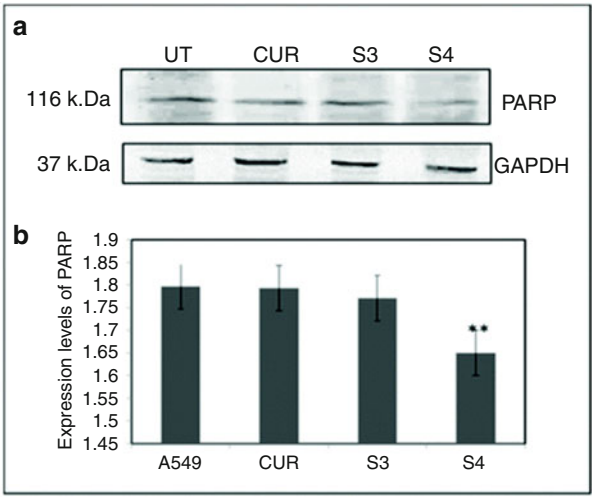

Fig. 11.13 Western blot analysis for poly ADP ribose polymerase (PARP) expression in A549 cells. (**a**) Immunoblotting shows the downregulation of the PARP levels in cells treated with **S4** compared to untreated control cells, indicating the induction of apoptosis by the material. (**b**) The quantification of PARP expression with respect to GAPDH is presented as a histogram. *P " 0.05, **P " 0.005 compared to control. (Adapted from Ref. [36]. Copyright © 2016, Royal Society of Chemistry)

4.2.4 In Vivo Studies

To comprehend the practical validity of in vitro biological characterizations and therapeutic potential of nanoparticulate targeted DDSs, their in vivo characterization/experiments in animal models are highly essential. The in vivo studies employing DDSs generally include tumor regression analysis, biodistribution, histopathology, and immunohistochemistry. For instance, Sau et al. developed different AuNPs-based nanoformulations for cancer therapeutics application [41]. These nanoformulations included (F2) AuNPs-MDA (MDA: 11-mercaptoundecanoic acid), (F3) AuNPs-Dex (Dex: Dexamethasone), (F4) AuNPs-MDA-Dex, (F5) AuNPs-Dex MDA, as well as (F1) water-Dex-MDA formulation without AuNPs. Intraperitoneal administration of these formulations to melanoma tumor containing C57BL6/J mice showed that F5 significantly inhibited the tumor growth in comparison with other formulations and untreated (UT) control experiment, as observed by tumor regression analysis (Fig. 11.14a–c). Immunohistochemistry study of tumor sections of different groups also revealed that F5 induced more apoptosis as compared to UT and other formulations, as indicated by the TUNEL-based green fluorescence in the respective tumor section (Fig. 11.14d). Additionally, the biodistribution of AuNPs in F5-administered mice through ICP-MS showed higher entrapment of AuNPs in tumor than in other vital organs such as lungs, spleen, and kidney. The overall result suggested the cancer therapeutic potential of F5 nanoformulation.

The following section briefly discusses the experimental methodology of different in vivo studies. In case of targeted DDS for cancers, respective doses of DDS are administered through various routes (i.p.: intraperitoneal,. i.v.: intravenous, i.m.: intramuscular, intratumoral, and oral) to animals (e.g., mouse, rat, rabbit, and others) containing tumors for some certain days. The volume of the tumors are measured from starting day of experiment to sacrificing day to plot the regression of tumors that would give an overview of the therapeutic potential of the DDS [42].

Similar to cellular uptake experiment in vitro, nanoparticulate DDS could be characterized by in vivo biodistribution analysis either through ICP-OES/ICP-MS or in vivo imaging system. Various important organs (e.g., brain, heart, lung, liver, kidney, spleen, etc.) of animals are collected after sacrificing, followed by washing with DPBS and digested in nitric acid. The digested tissue solutions are subjected to ICP-OES/ICP-MS analysis to detect the availability of the DDSs with respect to the content of respective elements present in nanoparticles. On the other hand, sometimes DDS containing NIR dye might be administered to the animals for some time periods, and then after sacrificing the animals, the vital organs are analyzed through in vivo imaging system to understand the biodistribution of the DDS in different organs.

Histopathology is one of the common methods to understand the structural change of organs due to toxicity of any kind of materials [43]. Therefore, researchers often perform histopathology of different organs of animals administered with nanoparticulate DDS. In brief, after completion of experiment period, the vital organs of animals are collected, washed with DPBS, and fixed with PFA. The tissue samples are then embedded in paraffin, sectioned, and fixed on clean slides. The

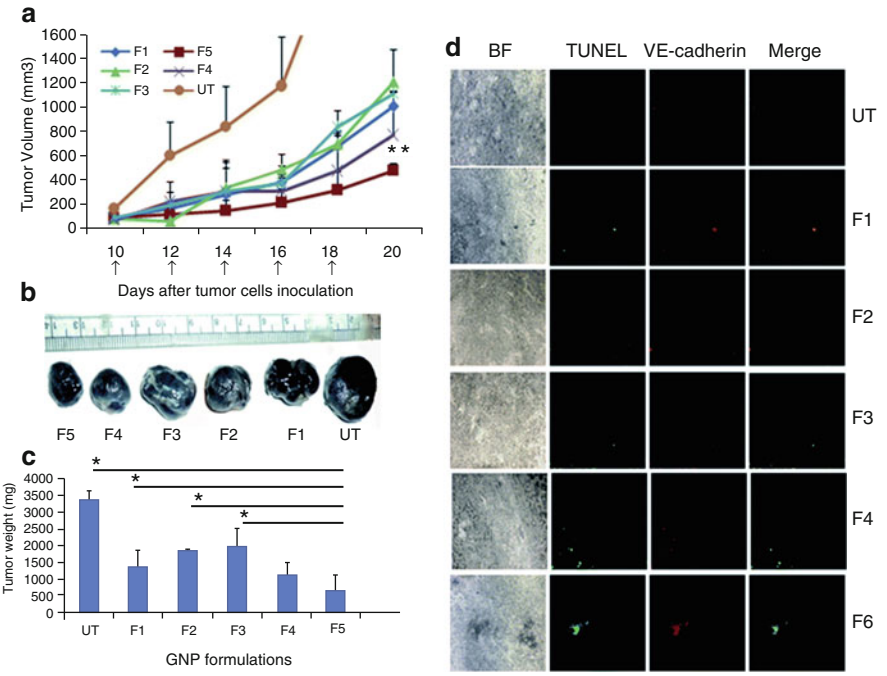

Fig. 11.14 Therapeutic study of GNP formulation: (**a**) tumor regression curve after subcutaneous implantation of B16F10 cells in C57BL6/J mice followed by intraperitoneal injection of F1–F5 or kept untreated (UT). Days of injection are indicated by black arrows. The dose of Dex in F1 was 10 mg kg^{-1}, whereas that in F3–F5 was 5 mg kg^{-1}. ** Denotes $p < 0.005$ for the F5 treatment with respect to the F1 treatment. (**b**) Representative tumors from mice of untreated group and different treated groups in the tumor model experiment (in vivo). (**c**) Comparison of average weight of isolated tumors from mice respectively treated with GNPs (F1–F5) or from the untreated (UT) group. * Denotes $p < 0.05$. (**d**) Microscopic pictures of 10 μm tumor sections from UT, and F1–F5 (upper to lower). Panels from left respectively indicate the tissue architecture in bright field (BF), apoptotic regions in TUNEL assay (green fluorescent), region with endothelial cells having VE-cadherin stained (red fluorescent) and merger (yellow) of the second and the third panels from the left. All the images are taken at 10× magnification. (Adapted from Ref. [41]. Copyright © 2016, Royal Society of Chemistry)

slides are dipped in xylene, rehydrated with ethanol, rinsed with water, and placed in hematoxylin solution. After that, the tissue slides are washed with acidic water, rinsed with 70% ethanol, and dipped in eosin solution, followed by dehydration using absolute ethanol. Finally, tissue slides are rinsed in xylene and mounted using mounting media followed by analyzing under bright-field microscope.

Similar to in vitro immunocytochemistry, in vivo tissue samples of animals administered with DDS are often analyzed through immunohistochemistry experiment to check the expression of proteins of interest. Briefly, the tissue samples are washed with DPBS, fixed with PFA, and rinsed with 20% glycerol. While

processing, the tissue samples are embedded in paraffin, sectioned, and fixed on clean slides. The tissue slides are dipped in isopropanol and xylene for few minutes and warmed in sodium citrate buffer. After cooling, the tissues are subjected to block with BSA in TBST buffer, followed by incubation with primary antibody and fluorescence moiety-tagged secondary antibody for few hours sequentially. Finally, the tissue samples are washed with TBST buffer and mounted with DAPI for nucleus staining. The tissue slides are then analyzed through fluorescence/confocal microscopy to comprehend the expression of the target proteins.

5 Therapeutic Applications of Drug Delivery Systems: Key Research Findings

Since past decades, scientists have developed various active and passive targeted nanoparticulate DDSs using different biocompatible nanoparticles, including gold, silver, zinc oxide, iron oxide, titanium dioxide, CNTs, CDs, and SiNPs. The following sections briefly discuss the therapeutic applications of few recent advancement of these nanomaterial-based DDSs.

5.1 Gold Nanoparticles

Over the past decades, AuNPs have been developed for a wide variety of applications including catalysis, bioanalysis, and imaging. But the most important application of AuNPs drawing attention to the researchers is the use of AuNPs as an ideal drug delivery scaffold because they are known to be nontoxic and nonimmunogenic. Researchers can readily functionalize the AuNPs with multiple targeting molecules and have shown their excellent potential for the delivery of various potential anticancer and antibacterial drugs. Several AuNPs-based drugs are currently under clinical trials [44, 45]. In the recent years, researchers are trying to develop various drug delivery platform based on AuNPs for better antitumor efficacy. In this context, a pH-responsive DDS has been developed by Aryal et al. [46] The authors have developed hydrophilic DOX-conjugated AuNPs, which exhibit a significant pH-responsive drug release. Thiolated methoxy polyethylene glycol (MPEG-SH) and methyl thioglycolate (MTG) at an equal molar ratio have been used to stabilize the AuNPs. The anticancer drug DOX has been attached to the MTG segments of the thiol-stabilized AuNPs through hydrazine as the linker. DOX-conjugated AuNPs have the potential to deliver the anticancer drugs to their target site to simultaneously enhance CT imaging contrast and facilitate photothermal cancer therapy. In another study, Brown et al. have functionalized naked AuNPs with a thiolated poly(ethylene glycol) (PEG) monolayer capped with a carboxylate group to tether the active component of the anticancer drug oxaliplatin for improved drug delivery [47]. The nanoparticle-conjugated drug shows as good as, or significantly better, cytotoxicity than oxaliplatin alone in all of the cell lines. It has also unusual ability to penetrate the nucleus in the lung cancer cells. Green

synthesis of AuNPs was achieved by Kumar et al. using the extract of eggplant as a reducing agent. HA serves as a capping and targeting agent [48]. Metformin (MET) was successfully loaded on HA-capped AuNPs (H-AuNPs), and this formulation binds easily on the surface of the liver cancer cells. This formulation exhibited better targeted delivery as well as increased regression activity than free MET in HepG2 cells. Suarasan et al. further developed a new pH- and temperature-responsive nanochemotherapeutic system based on DOX non-covalently bound to biosynthesized gelatin-coated gold nanoparticles (DOX-AuNPs@gelatin) [49]. The high drug loading capacity and effective drug release under pH control combined with the advantage of multimodal visualization inside cells clearly indicate the high potential of our DOX-AuNPs@gelatin delivery system for implementation in nanomedicine.

5.2 Silver Nanoparticles

Besides AuNPs, AgNPs are also extensively used as an effective drug delivery platform. For instance, Benyettou et al. demonstrated simultaneous intracellular delivery of DOX and alendronate (Ald) by bisphosphonate Ald-coated AgNPs (Ald@AgNPs) for improving the anticancer therapeutic indices of both drugs [50]. Dox- and Ald-loaded AgNPs (Dox-Ald@AgNPs) show better anticancer activity in vitro than either Ald or Dox alone. Ald@AgNPs nanoplatform can accommodate the attachment of other drugs as well as targeting agents and can be used as a general platform for drug delivery. Figure 11.15 represents the synthesis of Ald@AgNP and dye/drug conjugation, intracellular uptake of drug-Ald@AgNPs, and subsequent drug release. Intracellular release of drug occurred within the acidic microenvironment of late endosomes and lysosomes. In another study, Li et al. functionalized the surface of AgNPs by polyethylenimine (PEI) and paclitaxel (PTX) to evaluate the cytotoxic effect of Ag@PEI@PTX on HepG2 cells and corresponding anticancer mechanism [51]. It has been shown that Ag@PEI@PTX could enhance the cytotoxic effects on HepG2 cells and triggered intracellular reactive oxygen species. Further the signaling pathways of AKT, p53, and MAPK were activated to advance cell apoptosis. The result shows that Ag@PEI@PTX can be used as an appropriate candidate for chemotherapy of cancer. Liang et al. have further developed HA modified AgNPs for targeting CD44 receptors over-expressed cancer cell lines for targeted cancer therapy [52]. HA was used as the reducing agent and stabilizer and for targeting CD44. The antitumor efficacy was significantly improved by HA modification. Moreover, multiple mechanisms including the decline of mitochondrial membrane potential, cell-cycle arrest, apoptosis, and autophagy are involved for the enhanced anticancer activities of HA-AgNP, which provided a promising solution for AgNPs-mediated cancer treatment. In another study, Wang et al. proposed one-step synthesis approach for folic acid (FA)-coated AgNPs for DOX drug delivery [53]. Paramasivam et al. also reported biopolymers of chitosan (CH) and dextran sulfate (DS)-coated silver nanorods (AgNRs) for encapsulation of water-soluble antibacterial drugs like ciprofloxacin hydrochloride (CFH)

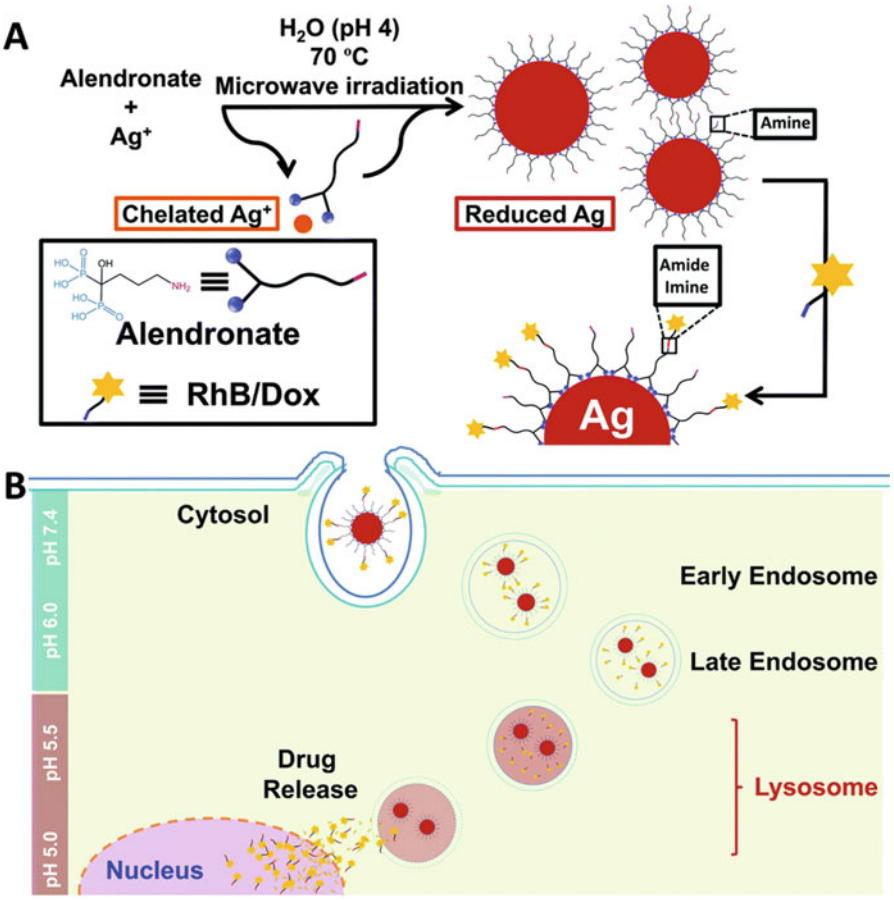

Fig. 11.15 (**a**) Schematic representation of Ald@AgNP formation and dye/drug conjugation. (**b**) Schematic representation of the uptake of drug–Ald@AgNPs into cells and drug cargo release. (Adapted from Ref. [50]. Copyright © 2015, Royal Society of Chemistry)

[54]. The authors compared the encapsulation of drugs and profiles of drug release to that of spherical AgNPs. Such system shows unique and attractive characteristics required for drug delivery.

5.3 Zinc Oxide Nanoparticles

Zinc oxide (ZnO)-based drug delivery platform has many advantages over the other DDSs as it is benign and weakly toxic. This property of ZnO nanoparticle makes it ideal for drug delivery application. In this context, Cai et al. developed a pH-responsive drug delivery platform for intracellular controlled release of drugs

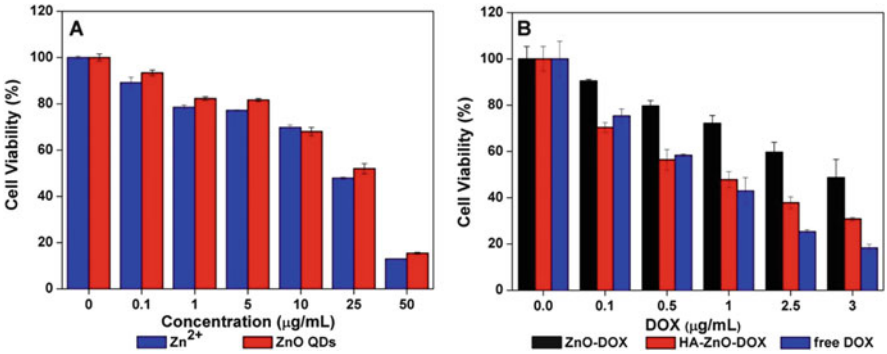

Fig. 11.16 Cytotoxicity assay of A549 cells after 48 h of incubation with (**a**) ZnO QDs and comparable concentrations of Zn^{2+} ions; (**b**) ZnO − DOX, HA − ZnO − DOX, and free DOX. (Adapted from Ref. [55]. Copyright © 2016, American Chemical Society)

based on acid-decomposable, luminescent-aminated ZnO quantum dots (QDs) [55]. NH_2-ZnO QDs are attached with dicarboxyl terminated PEG to increase their stability in physiological condition, followed by the attachment of a targeting ligand HA to target the CD44 over-expressed cancer cells. PEG-functionalized ZnO QDs are loaded with DOX via formation of metal-DOX complex and covalent interactions. Dissociation of the metal-drug complex and a controlled DOX release was occurred as pH-sensitive ZnO QDs dissolved to Zn^{2+} in acidic endosome/lysosome after cellular uptake, leading to achieve a synergistic therapy. Figure 11.16 represents the cytotoxicity of ZnO QDs and comparable concentrations of Zn^{2+} ion in human lung cancer (A549) cell line. The result showed that both displayed significant antitumor effect with the dosage surpassing 25 μg/mL. The cytotoxicity of ZnO-DOX, HA-ZnO-DOX, and free DOX was also evaluated in A549 cell line. Dose-dependent toxicity was found in all the three groups. Moreover, toxicity of HA-ZnO-DOX was higher than ZnO-DOX due to specific targeting of HA. In another study, an iron oxide–zinc oxide core-shell nanoparticle has been synthesized, which can deliver carcinoembryonic antigen into dendritic cells [56]. As a result, enhanced tumor antigen-specific T-cell responses delayed tumor growth and better survival was obtained in nanoparticle–antigen complex-treated mice, immunized with dendritic cells. In another report, Chen et al. synthesized core-shell structured NCs with ZnO QDs-conjugated AuNPs as core and amphiphilic block copolymer (containing poly l-lactide: PLA inner arm and a folate-conjugated sulfated polysaccharide outer arm) as shell for targeted anticancer drug delivery. Both NCs and CPT-loaded NCs show better antitumor efficacy in mice [57]. In another study, water-soluble curcumin was delivered by 3-mercaptopropionic acid (MPA)-functionalized ZnO-NPs. ZnO-MPA-curcumin complex shows enhance toxicity on MDA-MB-231 breast cancer cells compared to free curcumin, which suggests novel ZnO-MPA-curcumin

nanoformulation is promising and could be considered for new therapeutic application [58]. Further, Han et al. reported the targeted photocatalytic and chemotherapy in a multifunctional drug delivery platform based on aptamer-functionalized ZnO nanoparticles (NPs) [59]. Aptamer-ZnO NPs system loaded with anticancer drugs shows higher rate of death of cancer cells compared to that of single photocatalytic or chemotherapy. The results indicate the potential of aptamer-functionalized semiconductor nanoparticles for targeted photocatalytic and chemotherapy against cancer.

5.4 Iron Oxide Nanoparticles

Magnetic iron oxide (IO) nanoparticles are extensively used as a promising theranostic candidate for drug delivery. For example, Chen et al. showed the delivery of DOX by a reducible copolymer self-assembled with superparamagnetic iron oxide nanoparticles (SPIONs) [60]. rPAA@SPIONs were synthesized by the alkyl grafts of reducible copolymers made of polyamidoamine (rPAA) with PEG/dodecyl amine graft intercalated with the oleic acid layer capped on the surface of magnetite nanocrystals. rPAA@SPIONs loaded with anticancer drug DOX inhibited the tumor growth in mice with xenograft MDA-MB-231 breast tumor. In another study, Park et al. converted drug-loaded polymeric NPs into polymer iron oxide nanocomposites (PINCs) by dopamine polymerization for drug delivery application [61]. PINCs was accumulated in poorly vascularized subcutaneous SKOV3 xenografts that did not support the EPR effect by in vivo magnetophoretic delivery and showed better efficacy. Nasongkla et al. also developed iron oxide nanoparticle-based theranostic abbreviated as SPIO-DOX-cRGD micelles for targeted drug delivery. The authors loaded DOX and a cluster of magnetic iron oxide nanoparticles into the cores of PEG-PLA micelles, which was further functionalized with cRGD targeting ligand for targeting the integrin αvβ3 of tumor or endothelial cells. SPIO-DOX-cRGD micelles exhibited enhanced uptake in αvβ3 overexpressing endothelial cells [62]. In another study, Hwu group conjugated iron oxide nanoparticle surfaces by PTX, a mitotic inhibitor used in cancer chemotherapy, through a phosphodiester moiety to increase the efficacy of PTX [63]. Further, Quan et al. developed a human serum albumin (HSA)-coated iron oxide nanoparticles (HINPs) and loaded DOX onto the HINPs to assess the potential of the conjugate (D-HINPs) as theranostic agent [42]. D-HINPs showed a striking tumor suppression effect that was comparable to that of Doxil and greatly outperformed free Dox in a 4 T1 murine breast cancer xenograft model. Such a strategy can be readily applicable to other types of anticancer drugs, making HINPs a promising theranostic nanoplatform. Figure 11.17 represents the tumor growth inhibition study and body weight change by the treatment of D-HINPs in 4 T1 tumor model. The result shows the significant antitumor effect of D-HINPs, and it does not cause any toxicity to mice.

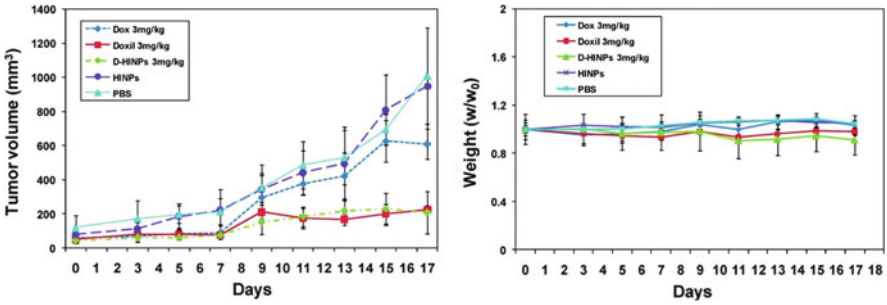

Fig. 11.17 Left: tumor growth curves for treatment with (1) D-HINPs (3 mg of Dox/kg); (2) free Dox (3 mg of Dox/kg); (3) Doxil (3 mg of Dox/kg); (4) HINPs (with same Fe concentration as in 1) and (5) PBS. D-HINPs showed similar therapeutic efficacy to Doxil and greatly outperformed free Dox. Right: change of mouse body weight during treatment (n = 5/group). (Adapted from Ref. [42]. Copyright © 2011, American Chemical Society)

5.5 Titanium Oxide Nanoparticles

Titanium oxide with its unique properties is found to be a potential candidate in drug delivery. For instance, Li et al. designed biocompatible one-dimensional titanium dioxide whiskers (TiO_2 Ws) loaded with daunorubicin (DNR) and explored it for drug delivery application and anti-tumor function [64]. Intracellular concentration and potential anti-tumor efficiency of DNR is greatly increased in presence of TiO_2Ws in human hepatocarcinoma cells (SMMC-7721 cells), indicating TiO_2Ws could produce an efficient drug delivery carrier effect importing DNR into target cells. This study reveals that TiO_2Ws-based delivery of anticancer drugs represents a promising approach in cancer therapy. Further, Kamari et al. prepared insulin conjugated montmorillonite nanocomposites, which were further coated with TiO_2 to modulate the slow release of insulin from the DDS [65]. The results showed that incorporation of TiO_2 coating significantly enhanced the drug loading, while reducing the amount of drug release, so that the nanocomposites without and with TiO_2 coating could release insulin after 60 min and 22 h at pH 7.4, respectively. The authors suggest that these findings could be used for converting the administration of insulin from injection to oral. In another study, graphene oxide/TiO_2/DOX (GO/TiO_2/DOX) composites was loaded into the chitosan/PLA solutions to synthesize the electrospun chitosan/PLA/GO/TiO_2/DOX nanofibrous scaffolds via electrospinning process for increasing the efficacy of DOX [66]. The higher sustained release rate of DOX following the small burst release was achieved from nanofibrous scaffolds having 30 and 50 m thicknesses within 2 weeks incubation time. It was also found that the DOX release rate is faster in pH 5.3 compared to pH 7.4. Higher proliferation inhibition effect of nanofibers on target lung cancer cells was observed in the presence of magnetic field. Wang et al. also introduced PEI-modified novel multifunctional porous titanium dioxide (TiO_2) nanoparticles to achieve ultraviolet (UV) light-triggered drug release [67]. Additionally, FA was chemically attached to the surface of the functionalized multifunctional porous TiO_2 nanoparticles through

amide linkage with free amine groups of PEI to effectively promote cancer-cell-specific uptake through receptor-mediated endocytosis. A typical poorly water-soluble anticancer drug PTX was incorporated in multifunctional porous TiO_2 nanoparticles and its drug delivery efficiency was studied. The anticancer effect was controlled by the amount of drug released from multifunctional porous TiO_2 nanoparticles regulating the UV-light radiation time. This multifunctional porous TiO_2 nanoparticle shows a combination of stimuli-triggered drug release and cancer cell targeting. Further, Leon et al. prepared a novel targeting DDS for 2-methoxyestradiol (2ME) for improving the clinical application of this antitumor drug [68]. For this purpose, TiO_2-PEG–2ME composite was formed, where 2ME was encapsulated in titanium dioxide (TiO_2) nanoparticle coated with PEG. Modifying TiO_2 NPs with PEG loaded with the 2ME drug showed that the titanium dioxide nanocarrier has potential application as a system of drug delivery.

5.6 Carbon Nanotubes

Among various nanomaterials, CNTs have drawn particular attention as carriers of biologically relevant molecules due to their unique physical, chemical, and physiological properties. For example, Chen et al. developed a novel single-walled carbon nanotube (SWNT)-based tumor-targeted DDS, consisting of a functionalized SWNT attached to tumor-targeting modules biotin and a spacer as well as prodrug, taxoid with a cleavable linker that is activated to its cytotoxic form inside the tumor cells upon internalization and in situ drug release [69]. It has been observed that this tumor-targeting DDS shows high potency toward specific cancer cell lines, thereby forming a solid platform for further development. In another study, Li et al. synthesized antibody of P-gp (anti-P-gp)-functionalized water-soluble single-walled carbon nanotubes (Ap-SWNTs) loaded with Dox, Dox/Ap-SWNTs, for overcoming the multidrug resistance (MDR) of K562 human leukemia cells [70]. The resulting Ap-SWNTs specifically recognize the multidrug-resistant human leukemia cells (K562R) and demonstrate controllable release performance for Dox toward the target K562R cells by near-infrared radiation (NIR) exposure. Dox/Ap-SWNTs showed 2.4-fold higher cytotoxicity and significant cell proliferation suppression toward K562R leukemia cells ($p < 0.05$) as compared with free Dox. Further, a dual-targeting DDS has been developed for treatment of brain glioma by Ren et al., based on PEGylated oxidized multiwalled carbon nanotubes (O-MWNTs) modified with angiopep-2 (O-MWNTs-PEG-ANG) [71]. O-MWNTs can distribute in brains, accumulate in tumors, and have ultrahigh surface area with remarkably high loading of anticancer drug DOX. Angiopep-2 can specifically combine to the low-density lipoprotein receptor-related protein (LRP) receptor overexpressed on the blood–brain barrier (BBB) and glioma cells, which was selected as targeting ligand. The antiglioma effect of DOX-loaded O-MWNTs-PEG-ANG (DOX-OMWNTs-PEG-ANG) was determined by C6 cytotoxicity and median survival time of glioma bearing mice, which revealed a better antiglioma effect than DOX, which suggests that O-MWNTs-PEG-ANG is a promising

dual-targeting carrier for brain tumor treatment. Further, Zhang et al. reported a pH-responsive targeted DDS based on single-wall carbon nanotubes (SWCNTs), functionalized with carboxylate groups and coated with a polysaccharide material [72]. Functionalized SWCNTs was loaded with the anticancer drug DOX at physiological pH (pH 7.4) and is only released in lysosomal pH and the pH characteristic of certain tumor environments. SWCNTs was also attached to FA, a targeting agent for many tumors for selective delivery DOX into the lysosomes of HeLa cells with much higher efficiency than free DOX. Meng et al. also reviewed the design and synthesis of SWNT-based DDSs and their pharmacokinetic, cancer targeting, and therapeutic properties both in vitro and in vivo [73].

5.7 Carbon Dots

CDs are exceptional nanocarriers due to their potential optical properties and biocompatibility. For instance, Feng et al. have reported a cisplatin (IV) prodrug conjugated CDs based extracellular micro-environment responsive DDS (CDs-Pt (IV)@PEG-(PAH/DMMA)) for imaging guided drug delivery [74]. High tumor inhibition efficacy and low side effects of cisplatin(IV) was observed in the presence of CDs nanocarrier, proving its capability as a smart drug nanocarrier with enhanced therapeutic effects. In another study, a smart stimuli-responsive DDS has been reported by Majumder et al. [75] Carbon-dot-coated novel alginate beads (CA-CD) was used as a drug delivery vehicle, in which garlic extract (GE), a model drug containing allicin, was loaded to form the DDS CA-CD-GE. The DDS exhibits pH-dependent controlled drug release which results in increased therapeutic efficiency. CA-CDGE is both stimuli responsive and a controlled drug release system as it releases drug according to the pathogen concentration (MRSA).

5.8 Mesoporous Silica Nanoparticles

In recent past, several research groups including ours have developed different MSN-based DDSs. For instance, Chen et al. developed dextrin-coated, DOX-conjugated MSNs-based DDS which could release DOX at a faster rate at mild acidic pH (pH 6.0) as compared to physiological (pH 7.4) [76]. The faster release of DOX at acidic pH might be due to the hydrolysis of Schiff's base (pH sensitive) present in the said DDS. Additionally, the in vivo studies in tumor (H22 cells)-bearing mice model illustrated the enhanced retention time and more entrapment of the DDS in tumor in comparison with pristine DOX, indicating the therapeutic efficacy of the DDS. In another report, M. B. Cardoso and group synthesized FA-modified SiNPs-based DDS containing anticancer drug curcumin [77]. The DDS exhibited efficient delivery of curcumin to prostate cancer cells (PC3). The authors further showed that the DDS was more cytotoxic to PC3 cells as compared to the prostate epithelial cell (PrEC), indicating the targeting efficacy of the DDS. Further, Palanikumar et al. reported a simple as well as robust procedure for the synthesis of

polymer (containing pyridine disulfide hydrochloride: PDS and PEG)-functionalized, targeting ligand (cyclic (Arg-Gly-Asp-D-Phe-Cys: cRGDfC)-decorated MSN-based DDSs containing hydrophilic anticancer drugs doxorubicin hydrochloride or cisplatin [78]. Here, PEG on MSN surface facilitated the water solubility and could prevent the nonspecific interaction with different biomacromolecules. On the other hand, PDS augmented the functionalization of the targeting ligand on MSN surface. The DDS exhibited high drug loading capability with 44 wt% for doxorubicin hydrochloride and 33 wt% for cisplatin. The results depicted that doxorubicin hydrochloride-conjugated polymer-wrapped MSNs (PMSNs) containing cRGDfC ligand (RGD-PMSNs) exhibited better cytotoxicity in KB cells (human nasopharyngeal carcinoma cells) as compared to the nonligand-wrapped PMSNs, indicating targeting efficacy of the DDS. Additionally, while both cisplatin- and Dox-loaded PMSNs were administered to KB cells, their synergistic effect showed better cytotoxic potential as compared to the treatment with single drug-loaded DDS, suggesting the potential applications of PMSNs for combination therapy. In another study, MSNs were used as a drug carrier for various hydrophobic anticancer drug (DOX, PTX, camptothecin: CPT, tamoxifen: TMX, Cur: curcumin), having high drug loading capability and colloidal stability [79]. The results illustrated that the combination of DOX-CPT-PTX and DOX-CPT-Cur with polymer-coated MSNs (PMSNs) showed better cytotoxicity to KB cells as compared to the DDS with single drug loading. Moreover, targeting ligand (RGD peptide: KB cells; SP94 peptide: HepG2 hepatocellular carcinoma cells) containing CPT-loaded PMSNs exhibited better cytotoxic potential and cellular uptake as compared to the nonligand-decorated PMSNs, suggesting the targeting efficacy of DDSs. Very recently, Oh et al. have developed GSH-modified anticancer drug (DOX and CPT)-loaded MSNs, decorated with HER2-binding affibody combined with glutathione-S-transferase (GST), to form a protein corona shielding nanoparticle (PCSN)-based targeted DDSs [80]. The affibody served as the targeting moiety as well as it could prevent the protein corona formation around the nanoplatform. Confocal microscopy study in Raw264.7 cells showed that the protein corona shield minimized the cellular uptake of PCSN in macrophages as compared to the PEGylated MSN (PEG-MSN). Further, confocal microscopy revealed that CPT-conjugated PCSN exhibited significant cytotoxicity to HER2 receptor over-expressing SKBR3 breast cancer cells as compared to HER2 receptor negative cells HEK293T, suggesting the targeting efficacy and potential application of the DDS for breast cancer therapy. To assess the in vivo biodistribution, the authors administered DiD-loaded PCSN and PEG-MSN to SKBR3 tumor-bearing nude mice intravenously. Post 48 h of injection, the mice were sacrificed and the vital organs were collected, followed by analysis through in vivo imaging system. The result exhibited that fluorescence intensity for PCSN group was significantly higher in tumor as compared to PEG-MSN group (Fig. 11.18a–b). Moreover, for PEG-MSN group, no such difference in fluorescence intensity between tumor and reticuloendothelial systems (liver and spleen) was observed. However, PCSN group exhibited almost seven times higher fluorescence signal in tumor than that in reticuloendothelial systems. The result suggested that the protein corona shielding could facilitate the

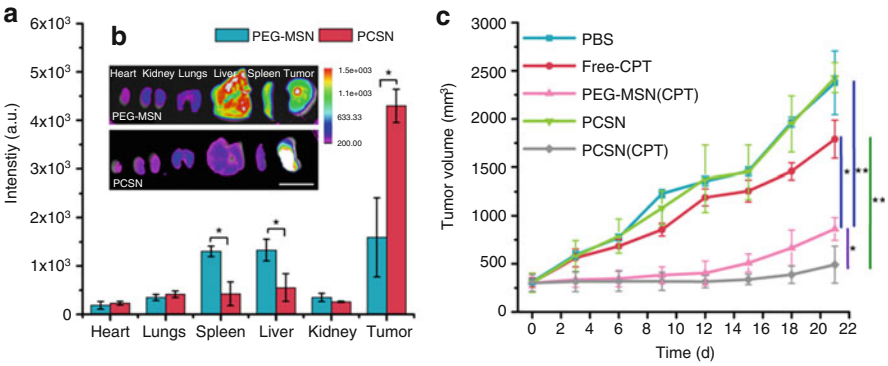

Fig. 11.18 Ex vivo and in vivo efficiency of PCSN. (**a**, **b**) Fluorescence images of organs and tumors 48 h after intravenous injection and biodistribution of injected formulations in animals with SK-BR3 tumor xenograft from fluorescence intensity analysis. In vivo antitumor effects in different treatment groups loaded with camptothecin (CPT) (1.5 mg/kg of mice) (scale bar is 2 cm). (**c**) Growth curve of tumor volume after intravenous injection with various groups of carriers until day 21 (n = 6 mice per group, mean ± 1 day [n = 6 mice per group, mean ± SD, statistical significance was calculated by one-way analysis of variance, $^{*}P < 0.05$, $^{**}P < 0.01$]. (Adapted from Ref. [80]. Open Access Journal)

nanoparticles to avoid immune system, thereby enhanced entrapment in target tumor site. Additionally, CPT-loaded PCSN (PCSN-CPT) exhibited better in vivo therapeutic efficacy as compared to CPT-loaded PEG-MSN and free CPT in terms of more tumor volume regression in SKBR3 tumor-containing mice (Fig. 11.18c). The overall experimental data demonstrated that binding of GST-HER2 affibody with MSNs leads to the formation of protein corona shield, which could minimize the interaction of PCSN with serum protein as well as improved its tumor targeting efficacy and therapeutic potential.

6 Conclusions: Challenges and Future Perspective

Since past decades, nanoparticulate targeted DDSs have been emerged as one of the revolutionizing nanomedicine approaches that could serve as an alternative to the conventional therapeutic treatment strategies for different diseases. Although, the study related to nanoparticulate targeted DDS have gradually been growing, the systematic investigation of nano-toxicity to humans is in early stage [81]. The physicochemical properties of nanomaterials such as size, morphology, surface charge, and stability often play a vital role behind their toxicological profile. To evaluate the nanotoxicity, the interaction of nanoparticles with cells, tissue, blood, proteins, and nucleic acids are to be thoroughly studied [82]. Additionally, number of doses of nanoparticulate system, administration route (i.p,. i.v., i.m., intramuscular, intratumoral, and oral), and immunological response are also to be assessed during the evaluation of toxicity profile of any nanomaterials. It is well known that

in vitro toxicity data of nanosystem might or might not be the similar in case of in vivo conditions. Therefore, in-depth evaluation of toxicological profile of nanoparticulate system is immensely important for the safety of our lives. Another challenge for nanomaterial-based system is that there is no precise uniform protocol for the assessment of toxicity of nanomaterials. It imposes the necessity for the development of standard protocols that would be followed globally, to get more reliable toxicity data for particular nanomedicine, which would be beneficial for practical biomedical applications of nanomaterials for human. Besides nanotoxicity, the fate of the nanomaterials for prolonged periods inside body system has to be considered for checking their adverse side effects. In this context, it is highly essential to investigate the pharmacokinetics, pharmacodynamics, and excretion of nanoparticulate systems. It is to be mentioned here that after investigating the thorough toxicological as well as pharmacokinetic profiles of therapeutic nanomaterials, the nanoformulations should be subjected to clinical trials, so that we could avail the practical benefits from the nanomedicines for different diseases. Although, there is not so much nanoparticulate targeted DDS available in market, considering the growth of present research in drug delivery field, we could expect many more nanomedicines would arise for practical biomedical applications for human in near future.

Acknowledgment This work was supported by the National Research Foundation of Korea (NRF) grant funded by the Korean Government (MSIP) (2016R1A5A1009405, 2017R1A2B4003617, and 2016R1E1A2A01954001).

References

1. Schaefer HE (2010) Nanoscience. The science of the small in physics, engineering, chemistry, biology and medicine. Springer Science+Business Media, Berlin
2. Teli MK, Mutalik S, Rajanikant GK (2010) Nanotechnology and nanomedicine: going small means aiming big. Curr Pharm Des 16:1882–1892
3. Dai L (2006) Carbon nanotechnology recent developments in chemistry, physics, materials science and device applications. Elsevier, Amsterdam
4. Khot LR, Sankaran S, Maja JM, Ehsani R, Schuster EW (2012) Applications of nanomaterials in agricultural production and crop protection: a review. Crop Prot 35:64–70
5. Lohse SE, Murphy CJ (2012) Applications of colloidal inorganic nanoparticles: from medicine to energy. J Am Chem Soc 134(38):15607–15620
6. Enterkin JA, Poeppelmeier KR, Marks LD (2011) Oriented catalytic platinum nanoparticles on high surface area strontium titanate nanocuboids. Nano Lett 11(3):993–997
7. Shipway AN, Katz E, Willner I (2000) Nanoparticle arrays on surfaces for electronic, optical, and sensor applications. ChemPhysChem 1(1):18–52
8. Han C, Andersen J, Pillai SC, Fagan R, Falaras P, Byrne JA, Dunlop PSM, Choi H, Jiang W, O'Shea K, Dionysiou DD (2013) Chapter green nanotechnology: development of nanomaterials for environmental and energy applications. In: Shamim N, Sharma VK (eds) Sustainable nanotechnology and the environment: advances and achievements, ACS symposium series, pp 201–229
9. Barui AK, Kotcherlakota R, Bollu VS, Nethi SK, Patra CR (2017) Biomedical and drug delivery applications of functionalized inorganic nanomaterials. In: Biopolymer-based

composites: drug delivery and biomedical applications. Woodhead Publishing, Copyright holder: Elsevier, Cambridge
10. Barui AK, Kotcherlakota R, Patra CR (2018) Medicinal applications of metal nanoparticles. In: Metal nanoparticles: synthesis and Applications in Pharmaceutical Sciences. Wiley-VCH Verlag GmbH & Co. KGaA, Weinheim
11. Winter JO (2007) Nanoparticles and nanowires for cellular engineering. In: Nanotechnologies for the Life Sciences. Wiley-VCH Verlag GmbH & Co. KGaA
12. Cho KJ, Wang X, Nie SM, Chen Z, Shin DM (2008) Therapeutic nanoparticles for drug delivery in cancer. Clin Cancer Res 14(5):1310–1316
13. Torchilin VP (2010) Passive and active drug targeting: drug delivery to tumors as an example. Handb Exp Pharmacol 197:3–53
14. Bae YH, Park K (2011) Targeted drug delivery to tumors: myths, reality and possibility. J Control Release 153(3):198–205
15. Danhier F, Feron O, Preat V (2010) To exploit the tumor microenvironment: passive and active tumor targeting of nanocarriers for anti-cancer drug delivery. J Control Release 148(2):135–146
16. Bhatia S (2016) Nanoparticles types, classification, characterization, fabrication methods and drug delivery applications. In: Natural polymer drug delivery systems. Springer International Publishing, Cham
17. Redhead HM, Davis SS, Illum L (2001) Drug delivery in poly(lactide-co-glycolide) nanoparticles surface modified with poloxamer 407 and poloxamine 908: in vitro characterisation and in vivo evaluation. J Control Release 70(3):353–363
18. Betancor L, Luckarift HR (2008) Bioinspired enzyme encapsulation for biocatalysis. Trends Biotechnol 26(10):566–572
19. Lee MY, Yang JA, Jung HS, Beack S, Choi JE, Hur W, Koo H, Kim K, Yoon SK, Hahn SK (2012) Hyaluronic acid-gold nanoparticle/Interferon α complex for targeted treatment of hepatitis c virus infection. ACS Nano 6(11):9522–9531
20. Reimer L, Kohl H (2009) Transmission electron microscopy physics of image formation, vol 51. Springer, New York, pp 1–15
21. Jores K, Mehnert W, Drecusler M, Bunyes H, Johan CKM (2004) Investigation on the stricter of solid lipid nanopartuicles and oil-loaded solid nanoparticles by photon correlation spectroscopy, field flow fractionasition and transmission electron microscopy. J Control Release 17:217–227
22. Molpeceres J, Aberturas MR, Guzman M (2000) Biodegradable nanoparticles as a delivery system for cyclosporine: preparation and characterization. J Microencapsul 17(5):599–614
23. Sanpui P, Chattopadhyay A, Ghosh SS (2011) Induction of apoptosis in cancer cells at low silver nanoparticle concentrations using chitosan nanocarrier. ACS Appl Mater Inter 3(2):218–228
24. zurMuhlen Z, zurMuhlen E, Niehus H, Mehnert W (1996) Atomic force microscopy studies of solid lipid nanoparticles. Pharm Res 13(9):1411–1416
25. Shi HQG, Farber L, Michaels JN, Dickey A, Thompson KC, Shelukar SD, Hurter PN, Reynolds SD, Kaufman MJ (2003) Characterization of crystalline drug nanoparticles using atomic force microscopy and complementary techniques. Pharm Res 20(3):479–484
26. Polakovic M, Gorner T, Gref R, Dellacherie E (1999) Lidocaine loaded biodegradable nanospheres II. Modelling of drug release. J Control Release 60:169–177
27. Liu Z, Robinson JT, Sun XM, Dai HJ (2008) PEGylated nanographene oxide for delivery of water-insoluble cancer drugs. J Am Chem Soc 130(33):10876–10877
28. Cui T, Liang JJ, Chen H, Geng DD, Jiao L, Yang JY, Qian H, Zhang C, Ding Y (2017) Performance of doxorubicin-conjugated gold nanoparticles: regulation of drug location. ACS Appl Mater Inter 9(10):8569–8580
29. Otsuka H, Nagasaki Y, Kataoka K (2003) PEGylated nanoparticles for biological and pharmaceutical applications. Adv Drug Deliver Rev 55(3):403–419
30. Palanikumar L, Kim J, Oh JY, Choi H, Park MH, Kim C, Ryu JH (2018) Hyaluronic acid-modified polymeric gatekeepers on biodegradable mesoporous silica nanoparticles for targeted cancer therapy. ACS Biomater Sci Eng 4(5):1716–1722

31. Kreuter J (1983) Physicochemical characterization of polyacrylic nanoparticles. Int J Pharm 14(1):43–58
32. Magenheim B, Levy MY, Benita S (1993) A new in-vitro technique for the evaluation of drug-release profile from colloidal carriers – ultrafiltration technique at low-pressure. Int J Pharm 94:115–123
33. Wang XY, Cai XP, Hu JJ, Shao NM, Wang F, Zhang Q, Xiao JR, Cheng YY (2013) Glutathione-triggered "off-on" release of anticancer drugs from dendrimer-encapsulated gold nanoparticles. J Am Chem Soc 135(26):9805–9810
34. Wang SH, Xu T, Yang YH, Shao ZZ (2015) Colloidal stability of silk fibroin nanoparticles coated with cationic polymer for effective drug delivery. ACS Appl Mater Inter 7(38):21254–21262
35. Bollu VS, Barui AK, Mondal SK, Prashar S, Fajardo M, Briones D, Rodriguez-Dieguez A, Patra CR, Gomez-Ruiz S (2016) Curcumin-loaded silica-based mesoporous materials: synthesis, characterization and cytotoxic properties against cancer cells. Mat Sci Eng C-Mater 63:393–410
36. Kotcherlakota R, Barui AK, Prashar S, Fajardo M, Briones D, Rodriguez-Dieguez A, Patra CR, Gomez-Ruiz S (2016) Curcumin loaded mesoporous silica: an effective drug delivery system for cancer treatment. Biomater Sci 4(3):448–459
37. Gayathri T, Barui AK, Prashanthi S, Patra CR (2014) Singh SP: meso-Substituted BODIPY fluorescent probes for cellular bio-imaging and anticancer activity. RSC Adv 4(88): 47409–47413
38. Barui AK, Nethi SK, Patra CR (2017) Investigation of the role of nitric oxide driven angiogenesis by zinc oxide nanoflowers. J Mater Chem B 5(18):3391–3403
39. Nagababu P, Barui AK, Thulasiram B, Devi CS, Satyanarayana S, Patra CR, Sreedhar B (2015) Antiangiogenic activity of mononuclear copper(ii) polypyridyl complexes for the treatment of cancers. J Med Chem 58(13):5226–5241
40. Modak A, Barui AK, Patra CR, Bhaumik A (2013) A luminescent nanoporous hybrid material based drug delivery system showing excellent theranostics potential for cancer. Chem Commun 49(69):7644–7646
41. Sau S, Agarwalla P, Mukherjee S, Bag I, Sreedhar B, Pal-Bhadra M, Patra CR, Banerjee R (2014) Cancer cell-selective promoter recognition accompanies antitumor effect by glucocorticoid receptor-targeted gold nanoparticle. Nanoscale 6(12):6745–6754
42. Quan QM, Xie J, Gao HK, Yang M, Zhang F, Liu G, Lin X, Wang A, Eden HS, Lee S, Zhang GX, Chen XY (2011) HSA coated iron oxide nanoparticles as drug delivery vehicles for cancer therapy. Mol Pharm 8(5):1669–1676
43. Mukherjee S, Dasari M, Priyamvada S, Kotcherlakota R, Bollu VS, Patra CR (2015) A green chemistry approach for the synthesis of gold nanoconjugates that induce the inhibition of cancer cell proliferation through induction of oxidative stress and their in vivo toxicity study. J Mater Chem B 3(18):3820–3830
44. Jain S, Hirst DG, O'Sullivan JM (2012) Gold nanoparticles as novel agents for cancer therapy. Br J Radiol 85:101–113
45. Libutti SK, Paciotti GF, Byrnes AA, Alexander HR, Gannon WE, Walker M, Seidel GD, Yuldasheva N, Tamarkin L (2010) Phase I and pharmacokinetic studies of CYT-6091, a novel pegylated colloidal gold-rhTNF nanomedicine. Clin Cancer Res 16(24):6139–6149
46. Aryal S, Grailer JJ, Pilla S, Steeber DA, Gong SQ (2009) Doxorubicin conjugated gold nanoparticles as water-soluble and pH-responsive anticancer drug nanocarriers. J Mater Chem 19(42):7879–7884
47. Brown SD, Nativo P, Smith JA, Stirling D, Edwards PR, Venugopal B, Flint DJ, Plumb JA, Graham D, Wheate NJ (2010) Gold Nanoparticles for the improved anticancer drug delivery of the active component of oxaliplatin. J Am Chem Soc 132(13):4678–4684
48. Kumar CS, Raja MD, Sundar DS, Antoniraj MG, Ruckmani K (2015) Hyaluronic acid co-functionalized gold nanoparticle complex for the targeted delivery of metformin in the treatment of liver cancer (HepG2 cells). Carbohydr Polym 128:63–74

49. Suarasan S, Focsan M, Potara M, Soritau O, Florea A, Maniu D, Astilean S (2016) Doxorubicin-incorporated nanotherapeutic delivery system based on gelatin-coated gold nanoparticles: formulation, drug release, and multimodal imaging of cellular internalization. ACS Appl Mater Inter 8(35):22900–22913
50. Benyettou F, Rezgui R, Ravaux F, Jaber T, Blumer K, Jouiad M, Motte L, Olsen JC, Platas-Iglesias C, Magzoub M, Trabolsi A (2015) Synthesis of silver nanoparticles for the dual delivery of doxorubicin and alendronate to cancer cells. J Mater Chem B 3(36):7237–7245
51. Li YH, Guo M, Lin ZF, Zhao MQ, Xiao MS, Wang CB, Xu TT, Chen TF, Zhu B (2016) Polyethylenimine-functionalized silver nanoparticle-based co-delivery of paclitaxel to induce HepG2 cell apoptosis. Int J Nanomedicine 11:6693–6702
52. Liang JM, Zeng F, Zhang M, Pan ZZ, Chen YZ, Zeng YN, Xu Y, Xu Q, Huang YZ (2015) Green synthesis of hyaluronic acid-based silver nanoparticles and their enhanced delivery to CD44(+) cancer cells. RSC Adv 5(54):43733–43740
53. Wang YL, Newell BB, Irudayaraj J (2012) Folic acid protected silver nanocarriers for targeted drug delivery. J Biomed Nanotechnol 8(5):751–759
54. Paramasivam G, Sharma V, Sundaramurthy A (2017) Polyelectrolyte multilayer film coated silver nanorods: an effective carrier system for externally activated drug delivery. In: IOP conference series: materials science and engineering, p 225
55. Cai XL, Luo YN, Zhang WY, Du D, Lin YH (2016) pH-Sensitive ZnO quantum dots-doxorubicin nanoparticles for lung cancer targeted drug delivery. ACS Appl Mater Inter 8(34):22442–22450
56. Cho NH, Cheong TC, Min JH, Wu JH, Lee SJ, Kim D, Yang JS, Kim S, Kim YK, Seong SY (2011) A multifunctional core-shell nanoparticle for dendritic cell-based cancer immunotherapy. Nat Nanotechnol 6(10):675–682
57. Chen T, Zhao T, Wei DF, Wei YX, Li YY, Zhang HX (2013) Core-shell nanocarriers with ZnO quantum dots-conjugated Au nanoparticle for tumor-targeted drug delivery. Carbohydr Polym 92(2):1124–1132
58. Ghaffari SB, Sarrafzadeh MH, Fakhroueian Z, Shahriari S, Khorramizadeh MR (2017) Functionalization of ZnO nanoparticles by 3-mercaptopropionic acid for aqueous curcumin delivery: synthesis, characterization, and anticancer assessment. Mater Sci Eng C 79:465–472
59. Han Z, Wang XH, Heng CL, Han QS, Cai SF, Li JY, Qi C, Liang W, Yang R, Wang C (2015) Synergistically enhanced photocatalytic and chemotherapeutic effects of aptamer-functionalized ZnO nanoparticles towards cancer cells. Phys Chem Chem Phys 17(33):21576–21582
60. Chen J, Shi M, Liu PM, Ko A, Zhong W, Liao WJ, Xing MMQ (2014) Reducible polyamidoamine-magnetic iron oxide self-assembled nanoparticles for doxorubicin delivery. Biomaterials 35(4):1240–1248
61. Park J, Kadasala NR, Abouelmagd SA, Castanares MA, Collins DS, Wei A, Yeo Y (2016) Polymer-iron oxide composite nanoparticles for EPR-independent drug delivery. Biomaterials 101:285–295
62. Nasongkla N, Bey E, Ren JM, Ai H, Khemtong C, Guthi JS, Chin SF, Sherry AD, Boothman DA, Gao JM (2006) Multifunctional polymeric micelles as cancer-targeted, MRI-ultrasensitive drug delivery systems. Nano Lett 6(11):2427–2430
63. Hwu JR, Lin YS, Josephrajan T, Hsu MH, Cheng FY, Yeh CS, Su WC, Shieh DB (2009) Targeted paclitaxel by conjugation to iron oxide and gold nanoparticles. J Am Chem Soc 131(1):66
64. Li QN, Wang XM, Lu XH, Tian HE, Jiang H, Lv G, Guo DD, Wu CH, Chen BA (2009) The incorporation of daunorubicin in cancer cells through the use of titanium dioxide whiskers. Biomaterials 30(27):4708–4715
65. Kamari Y, Ghiaci P, Ghiaci M (2017) Study on montmorillonite/insulin/TiO_2 hybrid nanocomposite as a new oral drug-delivery system. Mat Sci Eng C Mater 75:822–828

66. Samadi S, Moradkhani M, Beheshti H, Irani M, Aliabadi M (2018) Fabrication of chitosan/poly (lactic acid)/graphene oxide/TiO_2 composite nanofibrous scaffolds for sustained delivery of doxorubicin and treatment of lung cancer. Int J Biol Macromol 110:416–424
67. Wang TY, Jiang HT, Wan L, Zhao QF, Jiang TY, Wang B, Wang SL (2015) Potential application of functional porous TiO_2 nanoparticles in light-controlled drug release and targeted drug delivery. Acta Biomater 13:354–363
68. Leon A, Reuquen P, Garin C, Segura R, Vargas P, Zapata P, Orihuela PA (2017) FTIR and Raman characterization of Tio_2 nanoparticles coated with polyethylene glycol as carrier for 2-methoxyestradiol. Appl Sci 7(1)
69. Chen JY, Chen SY, Zhao XR, Kuznetsova LV, Wong SS, Ojima I (2008) Functionalized Single-Walled Carbon nanotubes as rationally designed vehicles for tumor-targeted drug delivery. J Am Chem Soc 130(49):16778–16785
70. Li RB, Wu R, Zhao L, Wu MH, Yang L, Zou HF (2010) P-Glycoprotein antibody functionalized carbon nanotube overcomes the multidrug resistance of human leukemia cells. ACS Nano 4(3):1399–1408
71. Ren JF, Shen S, Wang DG, Xi ZJ, Guo LR, Pang ZQ, Qian Y, Sun XY, Jiang XG (2012) The targeted delivery of anticancer drugs to brain glioma by PEGylated oxidized multi-walled carbon nanotubes modified with Angiopep-2. Biomaterials 33(11):3324–3333
72. Zhang XK, Meng LJ, Lu QH, Fei ZF, Dyson PJ (2009) Targeted delivery and controlled release of doxorubicin to cancer cells using modified single wall carbon nanotubes. Biomaterials 30(30):6041–6047
73. Meng LJ, Zhang XK, Lu QH, Fei ZF, Dyson PJ (2012) Single walled carbon nanotubes as drug delivery vehicles: targeting doxorubicin to tumors. Biomaterials 33(6):1689–1698
74. Feng T, Ai XZ, An GH, Yang PP, Zhao YL (2016) Charge-convertible carbon dots for imaging guided drug delivery with enhanced in vivo cancer therapeutic efficiency. ACS Nano 10(4):4410–4420
75. Majumdar S, Krishnatreya G, Gogoi N, Thakur D, Chowdhury D (2016) Carbon-dot-coated alginate beads as a smart stimuli-responsive drug delivery system. ACS Appl Mater Inter 8(50):34179–34184
76. Chen HY, Zheng DW, Liu J, Kuang Y, Li QL, Zhang M, Ye HF, Qin HY, Xu YL, Li C, Jiang BB (2016) pH-Sensitive drug delivery system based on modified dextrin coated mesoporous silica nanoparticles. Int J Biol Macromol 85:596–603
77. de Oliveira LF, Bouchmella K, Goncalves KD, Bettini J, Kobarg J, Cardoso MB (2016) Functionalized silica nanoparticles as an alternative platform for targeted drug-delivery of water insoluble drugs. Langmuir 32(13):3217–3225
78. Palanikumar L, Choi ES, Cheon JY, Joo SH, Ryu JH (2015) Noncovalent polymer-gatekeeper in mesoporous silica nanoparticles as a targeted drug delivery platform. Adv Funct Mater 25(6):957–965
79. Palanikumar L, Kim HY, Oh JY, Thomas AP, Choi ES, Jeena MT, Joo SH, Ryu JH (2015) Noncovalent surface locking of mesoporous silica nanoparticles for exceptionally high hydrophobic drug loading and enhanced colloidal stability. Biomacromolecules 16(9):2701–2714
80. Oh JY, Kim HS, Palanikumar L, Go EM, Jana B, Park SA, Kim HY, Kim K, Seo JK, Kwak SK, Kim C, Kang S, Ryu JH (2018) Cloaking nanoparticles with protein corona shield for targeted drug delivery. Nat Commun 9:4548
81. Elsaesser A, Howard CV (2012) Toxicology of nanoparticles. Adv Drug Deliver Rev 64(2):129–137
82. Xia T, Kovochich M, Liong M, Madler L, Gilbert B, Shi HB, Yeh JI, Zink JI, Nel AE (2008) Comparison of the mechanism of toxicity of zinc oxide and cerium oxide nanoparticles based on dissolution and oxidative stress properties. ACS Nano 2(10):2121–2134